INDEX

Astroparticle Physics 44 (2013) 68–75

Contents lists available at SciVerse ScienceDirect

Astroparticle Physics

journal homepage: www.elsevier.com/locate/astropart

Selecting gamma-ray showers from hadronic background using lateral shower age of EAS

R.K. Dey [a,*], A. Bhadra [b]

[a] Department of Physics, University of North Bengal, Siliguri, WB 734013, India
[b] High Energy and Cosmic Ray Research Centre, University of North Bengal, Siliguri, WB 734013, India

ARTICLE INFO

Article history:
Received 22 June 2012
Received in revised form 15 December 2012
Accepted 5 January 2013
Available online 12 January 2013

Keywords:
Cosmic ray
EAS
Lateral age
Local age
Simulation

ABSTRACT

A Monte Carlo (MC) simulation study has been carried out, aimed at identifying and rejecting the background component, constituted by hadronic cosmic rays, from γ-ray primaries in the multi-TeV region. In this work, our main focus is to discuss the possible role of the *local age parameter* (LAP) of cosmic ray extensive air shower (EAS) for separating γ-ray initiated showers from hadron initiated showers. Assigning a mean LAP to each EAS event, we found that the parameter might be useful for selecting γ-ray showers from hadron initiated showers in ground-based EAS experiments without muon measurement facilities.

1. Introduction

The present astrophysical conjecture of γ-ray astronomy leads to reflect newer concepts all the time in connection with the origin and acceleration mechanisms of cosmic rays (CRs). This becomes a viable branch of main stream astronomy with the advent of the ground-based imaging air Cherenkov telescopes (IACTs) [1]. The IACTs such as MAGIC [2], HESS [3], VERITAS [4] and the onboard Fermi Large area telescopes (FermiLAT) [5] along with the CGRO [6] produce results which agree remarkably well with the astrophysical model predictions. On the other hand, the imaging technique provides a method of effectively discriminating between γ-rays initiated showers and the background CR showers, based on the morphology of their Cherenkov images. To understand the important features of the primary energy spectrum vis-a-vis the chemical composition of the CRs at ultra high energy (UHE) and extremely high energy, a complete study of CR air-shower has been the only feasible way. The direct measurements of primary CR flux nearly 100 TeV and above are impractical because of very low and sharply falling flux, but has to be inferred from observations of extensive air showers.

The EAS measurements include estimation of various observable parameters namely shower size (N_e), muon size (N_μ), lateral shower age ($s_\perp$), local age ($s_{local}(r)$ or LAP), longitudinal age (s_L) of electron and muon distributions, hadron content (N_h), air shower associated Cherenkov photon content (N_{Ch}) and depth of shower maximum (X_{max}) (noticing that s_L and X_{max} measurements are made in air-shower arrays equipped with fluorescence detectors [7,8]) and most of these observables are found to be sensitive to primary masses with different degrees. To extract information about primary cosmic rays from the measurements of various experiments still require detailed MC simulations of the shower development as a basis of the data analysis and interpretation. The MC simulations consider the evolution of EAS in the atmosphere initiated by different energetic particles. Modern air-shower arrays equipped with large area detectors and improved electronics could precisely measure several EAS components simultaneously [9]. Employment of independent methods (or techniques) simultaneously using a hybrid detector set up to study high-energy CRs could help to limit systematic errors that have inundated CR experiments. The Pierre Auger Observatory uses hybrid detector in which those particles arriving at earth are detected through one technique while the other technique tracks the development of air showers by observing ultraviolet light emitted high in the earth's atmosphere [10]. Two or three detecting methods are also employed simultaneously in IceTop experiment in the south pole [11]. The inherently present shower-to-shower fluctuations in longitudinal development of EAS events corresponding to the same primary mass, energy and direction, measurements of EAS observables just providing important statistical information about the primary CRs.

In the field of CR air shower physics, the discrimination of γ-ray induced air showers from hadron-induced air showers is a chal-

* Corresponding author.
E-mail addresses: rkdey2007phy@rediffmail.com (R.K. Dey), aru_bhadra@yahoo.com (A. Bhadra).

0927-6505/$ - see front matter © 2013 Elsevier B.V. All rights reserved.
http://dx.doi.org/10.1016/j.astropartphys.2013.01.003

lenging problem that still needs more attention [12–14]. The high energy γ-rays are considered to be the by-product of hadronic components of primary CRs: a fraction of accelerated hadronic cosmic rays are likely to produce γ-rays through Δ-resonances, bremsstrahlung, inverse Compton etc. processes at or very close to the source site by interacting with the ambient matter [15]. The produced γ-rays will carry information about the origin of primary CRs as they point back at their source engines. The γ-ray detection suffers from the huge background constituted by ordinary CRs (hadrons) in the GeV–TeV energy region. The flux of primary γ-rays amongst the CRs has been estimated to be $\sim 10^{-5}$ of the proton flux at 100 TeV [16]. However, some early works predicted a Galactic plane excess higher than this: $\gamma/p \sim 10^{-3}, 3 \times 10^{-3}$ and 10^{-2} at $10^2, 10^3$ and 10^4 TeV [17]. Even at an energy of 10^7 TeV, this ratio has been predicted to rise up to 10^{-1} [18]. To observe astrophysical sources (emitting undeflected γ-rays and assumed as point-like objects) and to study the anisotropy properties of primary CRs, one has to eliminate isotropically distributed CRs.

Usually poor muon content is considered as the signature of γ-ray initiated EAS. In order to select a γ-ray shower based on such a criterion, an EAS array needs to be equipped with muon detectors covering very large area which is economically very challenging and such a facility is rarely available. So one has to look for some other primary mass sensitive observables based on which γ-ray initiated EASs can be separated out without the need of large area muon detector. In some early works, efforts were made to distinguish γ-ray showers on the basis of developmental stage of EAS in the atmosphere with the idea that γ-ray induced EAS will be younger than the hadron initiated EAS [19]. The lateral shower age ($s_\perp$), which is essentially the slope of the lateral density distribution of electrons in EAS (estimated by fitting the electron density data with the NKG function [20]) reflects the developmental stage of EAS and hence $s_\perp$ was used as distinguishing parameter. However, early MC simulation results regarding youthfulness of γ-ray induced showers in terms of shower age were inconclusive [21]. In those simulation works, authors used their own simulation codes and hence the findings could not be cross-checked. Since, nowadays standard simulation code like CORSIKA (COsmic Ray SImulation for KAscade) [22] is available and our knowledge about the high energy particle interactions is much improved now, it would be imperative to revisit the issue.

In the present work exploiting the CORSIKA MC simulation code, we made a detailed study on discrimination of γ-ray induced EAS from the large background contributed by hadrons in the multi-TeV range. The lateral shower profiles generated by various primaries within a particular primary energy range are being used here, and they provide some discriminatory power for separating γ-ray showers from the background. The selection of γ-ray initiated showers is attempted here by employing two different approaches - the Method I and the Method II. In the former approach (method I), we have taken single (r-independent) lateral age parameter i.e. $s_\perp$ as the γ-ray separation parameter. Besides, it has been argued in the literature that the different masses of primary CRs might also be separated using N_e, N_μ and f parameters [23]. The parameter f is giving out the ratio of reconstructed average electron densities at two arbitrary distance bands from the shower core, measuring roughly the rate of absorption of electrons in their lateral developments from the shower core. We also included this technique in the Method I. Experimentally it is observed that the NKG function with a single lateral age is insufficient to describe the lateral density distribution of EAS electrons properly at all distances, which implies that the lateral age changes with the radial distance. Subsequently, the notion of local lateral shower age parameter (LAP) was introduced [24] which is in essence the lateral age at a point. Since experimental electron density data in EAS may fluctuate considerably at a particular radial distance, instead of taking LAP at any particular point we take an average LAP between 50 m (where LAP is minimum) and 300 m (where LAP attains a local maximum) and in Method II, we employed this average LAP (s_{local}) to select γ-ray showers. It is found that when single constant lateral age ($s_\perp$) is used, the separation power becomes subdued. In contrast, the average LAP appears as a suitable mass sensitive parameter for classifying γ-ray induced showers.

The present study has been performed mainly at the geographical location of ARGO-YBJ (latitude 30.11°N, longitude 90.53°E, 4300 m a.s.l.) [25]. This is because the experiment offers a full coverage array and hence can measure radial density distribution of electrons in EAS with great accuracy, which in turn provides an opportunity to estimate LAP accurately. Moreover, since ARGO-YBJ does not have any muon detector, discrimination of γ-ray showers based on an alternative EAS observable, related to only electromagnetic component should be very useful. Since ARGO-YBJ experiment is located at very high altitude, its energy threshold is sub TeV and hence for this location we simulated EAS events in the energy range from 1 TeV to 3 PeV. However, ARGO-YBJ has not yet studied the radial variation of the lateral shower age while a few other experiments, such as Akeno [26] and NBU [27], successfully tested the predicted radial variation of LAP. We simulated a few events at the geographical location of Akeno and compared with the observations to demonstrate again the importance of considering LAP instead of single shower age. The correlations of $s_\perp$ with N_e and/or N_μ have been considered as a basis for extracting information on the nature of primary CRs. The KASCADE [28] and the NBU [29] experiments provide a few results on these aspects. Accordingly we performed simulations at geographical location of these experiments and compared with experimental findings in order to examine primary mass sensitivity of lateral shower age parameter. The MC simulation for generating EAS events considers interaction mechanisms of energetic particles as input. But due to the limited knowledge of particle interactions at high energies (and the large fluctuations) the results of simulation may become model dependent. To ensure that the conclusion of the present work is robust, we consider two high energy interaction models, QGSJet 01 v.1c [30] and EPOS – 1.99 [31] and found that the present findings do not have any strong dependence on the choice of interaction model.

The organization of the paper is as follows. The theoretical background of EAS age parameters $s_\perp$ and $s_{local}(r)$ described in the cascade theory is given in section 2. In section 3, the important considerations adapted in the simulation procedure are given. Estimation of lateral shower age and LAP is discussed in section 4. In sections 5 and 6, we present the results obtained on gamma-hadron separation employing method-I and method-II respectively. Finally, in section 7 summary and our conclusions are pointed out.

2. Shower age parameters: theoretical aspects

Extensive air showers propagating in the same density profile of the atmosphere essentially have equal lateral distributions around the shower axis. In the cascade theory, the problem of estimating the electron lateral distribution received an important recognition in the past. Nishimura and Kamata [32] solved numerically the 3-dimensional shower equations in *Approximation B* (electrons suffer constant amount of collision loss in a radiation length which is equal to the critical energy) to obtain the lateral distribution of electrons propagating in a medium of constant density. The results obtained on lateral density distribution of cascade particles by Nishimura and Kamata can be approximated by the well known Nishimura–Kamata–Greisen (NKG) structure function proposed by Greisen [20], given by

$$f(r) = C(s_\perp)(r/r_m)^{s_\perp - 2}(1 + r/r_m)^{s_\perp - 4.5}, \quad (1)$$

where the normalization factor C ($s_\perp$) is given by

$$C(s_\perp) = \frac{\Gamma(4.5 - s_\perp)}{2\pi\Gamma(s_\perp)\Gamma(4.5 - 2s_\perp)}. \quad (2)$$

The NKG formula has the advantage of normalization as it is integrable in Euler Beta function. The normalization of $f(r)$ implies for the electron density $\rho(r) = N_e f(r)$. But such a widely used relation does not hold if $s_\perp$ varies with r, as noted in Akeno [26], NBU [27] and some other observations [24]. An improvement of the NKG function was proposed by adopting a modulated, longitudinal age parameter s_L (the developmental stage of a pure electromagnetic cascade) dependent effective Moliere radius [33], so that,

$$\rho_{el}(r) = (mr_m)^{-2}\rho_{NKG}(r/m). \quad (3)$$

where r_m is the Moliere radius and $m = 0.78 - 0.21s_L$ so that mr_m may be referred as lateral age dependent effective Moliere radius. But even with such a modification, lateral shower age is found to vary with radial distance experimentally. To handle the situation a method was developed by Capdevielle et al. introducing the notion of *local age parameter* (LAP) [24]. From two neighboring points, i and j, we can give a LAP for any distribution $f(x)$ (where $x = \frac{r}{r_m}$) which characterizes the best fit by a NKG-type function in $[x_i, x_j]$:

$$s_{local}(i,j) = \frac{\ln(F_{ij}X_{ij}^2Y_{ij}^{4.5})}{\ln(X_{ij}Y_{ij})} \quad (4)$$

Here, $F_{ij} = f(r_i)/f(r_j)$, $X_{ij}=r_i/r_j$, and $Y_{ij}=(x_i+1)/(x_j+1)$. More generally, if $r_i \to r_j$, this suggests the definition of the LAP $s_{local}(x)$ (or $s_{local}(r)$) at each point:

$$s_{local}(x) = \frac{1}{2x+1}\left((x+1)\frac{\partial \ln f}{\partial \ln x} + 6.5x + 2\right) \quad (5)$$

Function $f_{NKG}(r)$ with $s=s_{local}(r)$ can be used to fit $f(r)$ in the neighborhood of r.

The identification $s_{local}(r) \equiv s_{local}(i,j)$ for $r = \frac{r_i+r_j}{2}$ remains valid for the experimental distributions (taking $F_{ij} = \rho(r_i)/\rho(r_j)$) as far as they are approximated by monotonic decreasing functions versus distance.

The behavior of LAP on experimental lateral distributions was found in accordance with the prediction [34] which was reaffirmed by the Akeno observations [26]. The stated method was validated by the rapporteurs of the ICRC from 1981 to 1985 [35]. In the present work, we have given emphasis on the estimation of the LAP and on its average using $s_{local}(r)$ values, taken between first minimum and the subsequent maximum from the radial variation of LAP. The estimation of $s_\perp$ would also be made through the traditional shower reconstruction method (electron density data are fitted with the NKG structure function over the entire radial distance under consideration).

3. Simulation of EAS

The EAS events are simulated by coupling the high energy (above 80 GeV/n) hadronic interaction models QGSJet 01 version 1c [30] and EPOS 1.99 [31], and the low energy (below 80 GeV/n) hadronic interaction model GHEISHA (version 2002d) [36] in the framework of the CORSIKA Monte Carlo program version 6.970 [37]. For the electromagnetic part the EGS4 [38] program library has been used. The US-standard atmospheric model [39] with planar approximation has been considered which works only for the zenith angle of the primary particles less than 70°. The maximum zenith angle of primaries has been restricted to 45° here.

The MC simulation data library consists of over 0.1 million EAS events each for p, Fe and γ-ray at the ARGO-YBJ location (latitude 30.11° N, longitude 90.53°E, 4300 m a.s.l.) in the primary energy range 1 TeV to 3 PeV using both QGSJet and EPOS models. In addition, we have generated 25,000 EAS events for each primary component p, Fe, and γ-ray and about 10,000 He events with the model QGSJet 01 v.1c in the primary energy range from 100 TeV to 30 PeV following a power law with a spectral index of −2.7 below the knee and −3.0 above the knee at the geographical locations of KASCADE (latitude 49.1° N, longitude 8.4° E, 110 m a.s.l.) and NBU (latitude 26.8° N, longitude 88.4° E, (~130 m a.s.l.). Besides, a small sample of events for p and Fe primaries are generated at the location of Akeno (35.78° N, 138.5° E, 900 m a.s.l.). The magnetic fields are set for all three observational levels accordingly.

Two mixed samples have been prepared from the generated showers taking 50% p, 25% He, 25% Fe events (mixture-I) and 37% p, 37% Fe, 26% γ-ray events (mixture-II) respectively for better understanding of EAS observational results.

4. Estimation of lateral shower age

The simulated electron density data have been analyzed in two different methods to obtain shower age parameters $s_\perp$ and $s_{local}(r)$. First, following the traditional approach we estimate $s_\perp$ (along with other shower parameters) by fitting the density data with the NKG structure function. In this approach, the simulated electron densities at different radial distances have been fitted by the method of chi-square minimization through an iterative procedure based on the method of steepest decent to the NKG lateral distribution function of electrons. Here it is to be noted that majority of the EAS groups generally estimate basic shower parameters based on the NKG function. In order to check the goodness of the NKG function in describing the simulated radial density distribution of electrons, we firstly fitted the simulated density data at various radial distances with the NKG function and compared radial density distribution of electrons for simulated events with the fitted curve. Fitted showers with reduced χ^2 less than 5 are only accepted for results involving $s_\perp$. The error in estimating $s_\perp$ in the N_e range $1.5 \times 10^4 - 4.25 \times 10^5$ has been found as ±0.03.

Secondly, exploiting Eq. (4) we directly estimated LAP for each individual event. We noted that the description of the data by the NKG function is improved when the Moliere radius is treated as a variable rather than a fixed parameter [40]. But this better description comes at the expense of very high shower age value which somewhat obscures the physical meaning of the age parameter as assigned in the cascade theory. In this analysis, the error of the LAP for EAS with the primary energy in the PeV range remains within 0.05 for 10 m < r < 250 m, whereas for r < 10 m or when r > 300 m the error of the LAP is found to be higher, about 0.1.

It has been shown recently [40] that LAP initially decreases with radial distance, reaches a minimum around 50 m, then starts increasing with radial distance, attains a local maximum around 300 m and decreases again thereafter. The nature of such a variation of LAP with radial distance was found independent of energy of the shower initiating particles [40]. We observed such a characteristic variation of LAP with radial distance at ARGO-YBJ location as shown in Fig. 1a for proton, iron and γ-ray primaries. It is seen from the Fig. 1a that the nature of variation is nearly the same for both QGSJet and EPOS. Here, it is worthwhile to mention that up to 50 TeV or so, the density of electrons in EAS beyond 50 m from the shower core is extremely small even at ARGO-YBJ level and is almost impossible to measure it in practical situation. Hence, we have chosen the primary energy from 100 TeV and above for results.

As already mentioned, Akeno group studied the radial variation of LAP experimentally [26]. We compared our simulation results with Akeno observations in Fig. 1b for proton and Fe primaries. The single lateral shower age for proton and iron primaries are also given (solid and dashed lines parallel to the x-axis) in the figure for

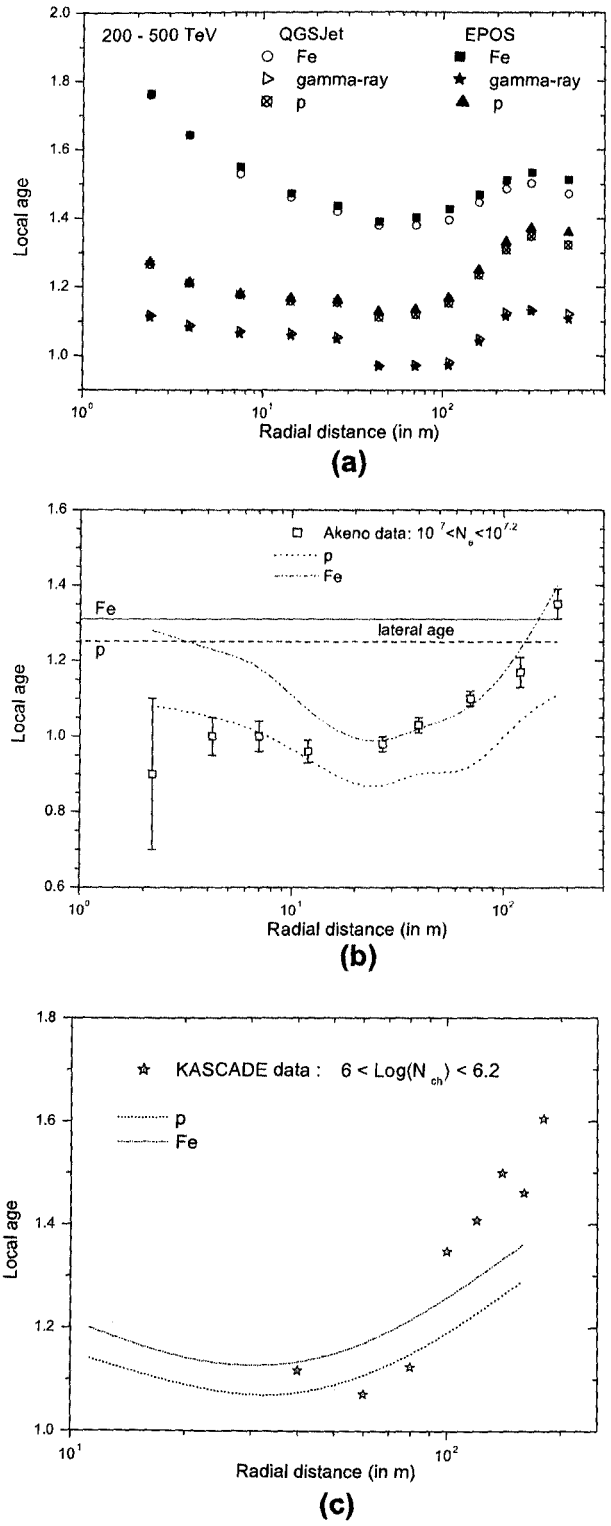

Fig. 1. (a) The radial variation of LAP obtained at the ARGO-YBJ altitude for p, Fe and γ-ray with hadronic interaction models QGSJet and EPOS. (b) Same as Fig. 1a at the Akeno level with QGSJet model, compared with experimental data. The solid and dashed lines parallel to the x-axis indicate $s_\perp$ for Fe and p. (c) The radial variation of LAP estimated from the KASCADE observed lateral distribution data. Lines indicate the mean values of a sample of simulated EAS events with QGSJet model (the errors in experimental data are not included here).

comparison. We also estimated LAP from the lateral density distribution of electrons obtained by the KASCADE experiment [28,41,42] and we compared with our simulation results in Fig. 1c. The errors in the extracted experimental points are quite large but it is at least clear that a constant single lateral shower age is insufficient to describe the experimental findings.

Since air shower measurements are subjected to large fluctuations, instead of LAP at a particular radial distance we consider for each event a mean LAP ($< s_{local} >$), which is the average of LAPs for several small distance bands (r_i, r_j) over the radial distance between 50 m to 300 m. For the purpose of averaging, distance bands are taken in constant steps on the logarithmic scale. The radial distance band from 50 m to 300 m is chosen because the positions of local minimum and maximum at 50 m and 300 m band are nearly universal, independently of primary energy [40].

5. Results on gamma-hadron separation: Method I

First, we analyzed the simulated EAS events generated at NBU and KASCADE locations (both at sea level), obtained $s_\perp$ and other shower parameters and compared with some of the published results of NBU [43] and KASCADE [28] respectively. Secondly, EAS events generated at the geographical location of ARGO-YBJ [25] are analyzed and both $s_\perp$ and $s_{local}(r)$ are estimated.

5.1. N_e & N_μ dependencies of $< s_\perp >$

The correlation between the mean lateral shower age ($< s_\perp >$) over a small shower size bin in the range ($10^3 - 1.5 \times 10^6$), with the zenith angle interval ($0^\circ - 45^\circ$) for p, Fe, γ-ray, mixed composition (mixture-I) using QGSJet model and corresponding NBU results [43] are put on view in Fig. 2a. The NBU EAS experiment reported the total uncertainties (including instrumental uncertainty) in estimating $s_\perp$ and N_e as $\pm 9\%$ and $\pm 0.14 N_e$ [29]. It is important to perceive that the lateral shower age takes higher values for heavy nuclei compared to that of light and γ-ray primaries clearly indicating relatively flatter lateral distribution of electrons as one moves from γ-ray to Fe via p.

The variation of $\langle s_\perp \rangle$ with muon size in the primary energy range ($10^2 - 3 \times 10^4$ TeV) and zenith angle interval ($0^\circ - 45^\circ$) for p, Fe, γ-ray primaries is presented in Fig. 2b with KASCADE data [28]. The variation exhibits the same nature as obtained in the KASCADE experiment using NKG fitting for muons with slightly higher muon threshold energy. The Fig. 2b exhibits the fact that γ-ray initiated showers can be separated out from the background using $\langle s_\perp \rangle$ and N_μ. It was also concluded in one of our previous work that EASs due to light primary components are younger on the average [40].

The KASCADE data points indicate that the composition changes slowly from predominantly proton at around 10^{14} eV to heavier primaries with the increase of energy. The NBU data are available only over a small energy window and though both the NBU and the KASCADE data suggest for a mixed composition in the common energy range of study, the NBU data favor for a relatively heavier composition. However, being a small EAS array the NBU experiment could measure electron density only up to 80 m from the shower core and its resolution power for primary composition is thus limited.

5.2. Variation of f with $\frac{N_\mu}{N_e}$

The lateral structure of EAS from different primaries attributes some power of identification and rejection of hadron primaries from γ-rays with the same primary energy and size [23]. From the lateral profile of each simulated EAS, we have estimated elec-

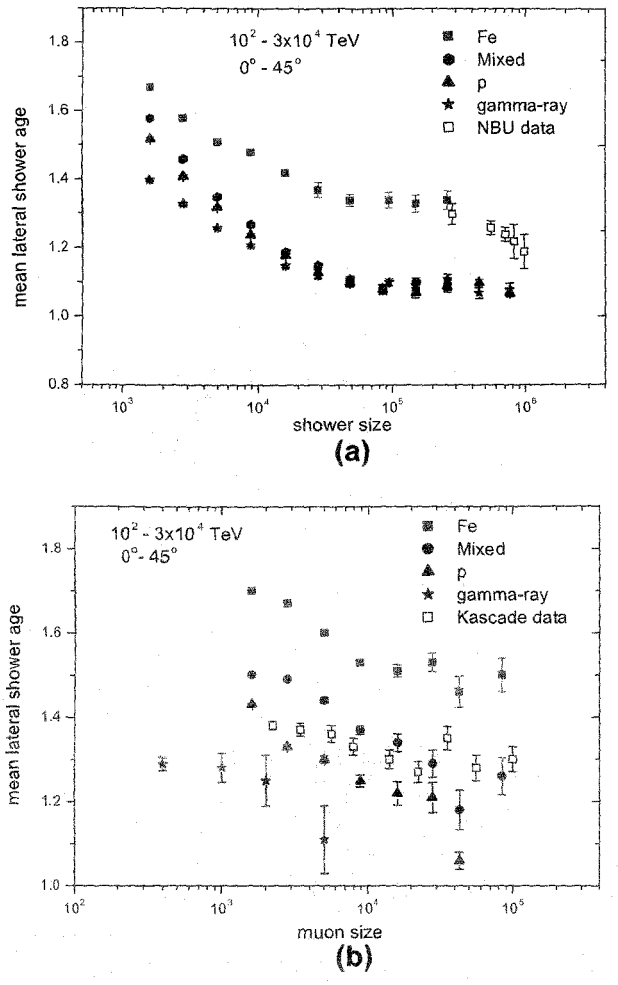

Fig. 2. (a) Variation of mean lateral shower age with shower size along with NBU data; (b) Variation of mean lateral shower age with muon size. For comparison with KASCADE data in Fig. 2b, where the age parameter was estimated by NKG fits with r_μ as 420 m and also used truncated muon sizes N_μ^{tr}. The QGSJet model has been used for simulation.

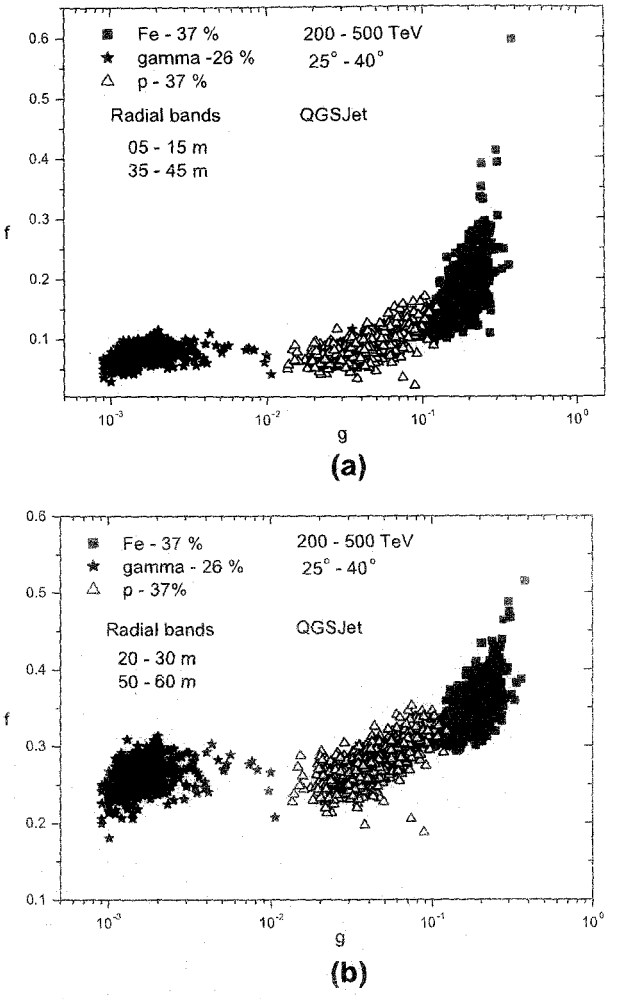

Fig. 3. Distribution of 200–500 TeV EAS events in the g-f plane at ARGO-YBJ level: (a) The ratio (f) for two electron densities are taken between distance bands (5–15) m and (35–45) m; (b) same as Fig. 3a but distance bands are taken at (20–30) and (50–60) m respectively. A negligible percentage of γ-ray primaries are found behind hadron (proton) showers.

tron densities at five adjacent radial points in each of the two arbitrarily chosen distance bands (5–15) m and (35–45) m. Next by employing the reconstruction procedure for the determination of local electron density (LED), we obtained two average reconstructed LEDs ρ_1 and ρ_2 from the shower core.

The selection of γ-ray showers from hadrons becomes visible when one plots the parameter f against g where $g = \frac{N_\mu}{N_e}$ as presented in a 2-dimensional Fig. 3a. The same study has been repeated for another pair of radial bands (20–30) m and (50–60) m, using the same sample of mixture-II and it is depicted in Fig. 3b. The rate of absorption of electrons decreases with increasing radial distance from the core and this feature is revealed from the comparison of Figs. 3a and 3b. We have checked that the characteristic feature of the $g - f$ distribution does not change appreciably for the high energy interaction model EPOS and for a different primary energy range (100–200) TeV.

It appears from the Fig. 3 that this technique essentially exploits the total muon content in an EAS. The events are classified according to their primaries along x-axis (the ratio of muon size to electron size is plotted along x-axis); there is no notable separation along y-axis between events generated by photons and protons.

6. Results on gamma-hadron separation:Method II

In this section we would explore through MC simulation study whether LAP is sensitive on primary mass and consequently the possible role that the parameter may play for separating γ-ray showers from a large background constituted by hadronic showers in primary CRs.

6.1. Variation of LAP with shower size

Due to overwhelming background from hadron induced EAS, the discrimination of the rare gamma-like events is vital. In Fig. 4 we have shown the variation of $< s_{local} >$ as a function of N_e for the primaries p, Fe, and γ-rays from simulated results. Please note that EAS events were simulated for the same fixed primary energy range irrespective of nature of primaries and since different primaries having the same energy may produce different N_e, in Figs. 4a and 4b the starting and ending values of N_e are not always the same for all the primaries. We considered a particular N_e region where data for all the primaries are more or less available with rea-

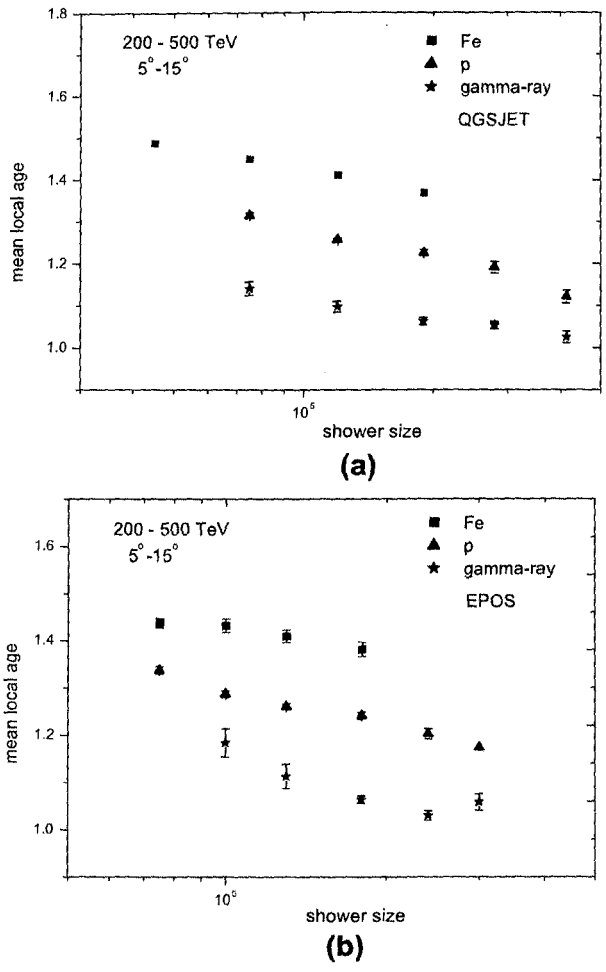

Fig. 4. (a) Variation of $< s_{local} >$ with N_e at ARGO-YBJ with QGSJet model; (b) same as Fig. 4a but for the model EPOS.

sonable statistics. It is clear from the plots that EAS events are classified according to their primaries along y-axis which means that γ-ray induced showers can be separated out on the basis of $< s_{local} >$. The scatter plots for the same variation are shown in Figs. 5a 5b and 5c where distribution of different primary masses based on s_{local} and N_e data from the mixture-II corresponding to different primary energies and interaction models are presented.

6.2. Selection of γ-ray component using LAP

In the primary CR flux, the percentage of γ-ray flux is very very small, of the order of 0.001%. To separate such a small fraction of γ-ray component from primary CRs in a real experiment employing method II, it would be nice if we could prepare a mixture with such a small percent of γ-rays and see whether the γ-ray events can be extracted out or not. But due to limited statistics we could not do that. Instead, we made three sub-mixtures of type II maintaining the ratio of primaries as 37% p, 37% Fe and 26% γ-ray for three different combinations of zenith angle, primary energy and shower size ranges. These exercises are done for both the high energy interaction models QGSJet and EPOS. From each sub-mixture, we tried to separate γ-ray showers out exploiting s_{local} corresponding to different N_e.

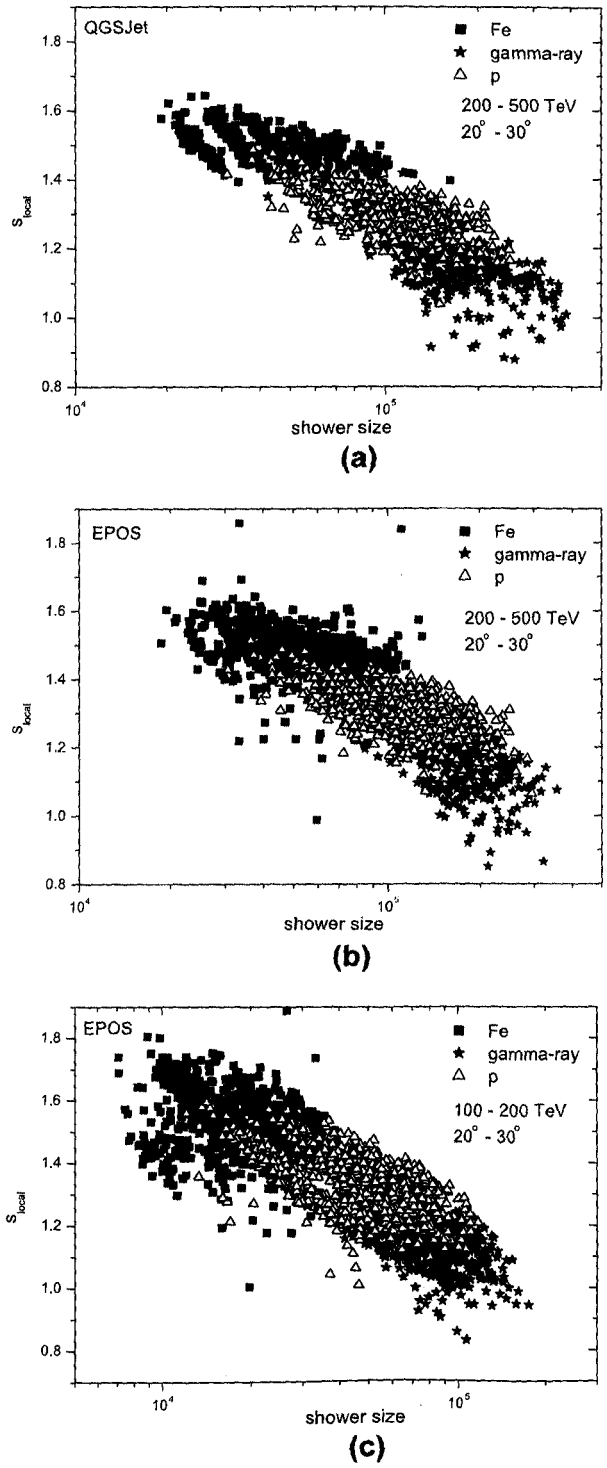

Fig. 5. (a)–(c) Distribution of simulated events in mixture-II in two primary energy ranges based on s_{local} and N_e at ARGO-YBJ. Dependence on interaction models is also shown.

For a small enough cut value of s_{local} we have found poor acceptance for γ-ray induced EAS and very good rejection of background, whereas for a large enough value of s_{local} the situation is found to be completely reversed. Cut values of s_{local} lie between the two ex-

Table I
The quality factor at various s_{local} cuts using QGSJet model. The primary energy, zenith angle and shower size intervals are (200–500) TeV, 20°–30° and (1.5–4.0) × 10^5, respectively.

s_{local}	1.05	1.08	1.10	1.12	1.14	1.15	1.16	1.18	1.20
ϵ_γ	0.146	0.237	0.348	0.510	0.657	0.707	0.778	0.864	0.934
ϵ_{bkg}	0.007	0.022	0.029	0.036	0.058	0.065	0.109	0.145	0.254
Q	1.74	1.61	2.05	2.69	2.73	2.77	2.36	2.27	1.86

Table II
The signal selection parameters at optimal conditions.

Model	E (TeV)	θ (deg.)	$N_e \times 10^5$	s_{local}	ϵ_γ	ϵ_{bkg}	Q
EPOS	100 – 200	5 – 15	0.6 – 2.0	1.14	0.691	0.072	2.57
EPOS	200 – 500	20 – 30	1.5 – 4.0	1.15	0.734	0.048	3.35
QGSJet	200 – 500	20 – 30	1.5 – 4.0	1.15	0.707	0.065	2.77

tremes offered different acceptances and rejections of γ-ray and background respectively. Similarly a proper cut on N_e is also needed for selection of γ-ray induced EAS and the rejection of background. In astronomical signal selection, optimal cut to selection parameters (maximizing the γ-ray efficiency and minimizing the background contamination) is usually set by numerical maximization of the quality factor Q defined by

$$Q = \frac{\epsilon_\gamma}{\sqrt{\epsilon_{bkg}}} = \frac{\epsilon_\gamma}{\sqrt{(1-\xi_{bkg})}} \tag{6}$$

where ϵ_γ and ϵ_{bkg} respectively denote the acceptances of γ-ray and background from the sample using a cut value of s_{local} but ξ_{bkg} stands for the rejection of background. Here, $\epsilon_\gamma = \frac{n_\gamma(cut)}{n_\gamma}$ and $\epsilon_{bkg} = \frac{n_{bkg}(cut)}{n_{bkg}}$, with $n_\gamma(cut)$ and $n_{bkg}(cut)$ represent number of showers of either kind those passed through a particular cut value of s_{local} while n_γ and n_{bkg} are the total number of showers present in the sample before the applied cut. Q essentially quantifies the gain of significance achieved by the separation algorithm. The quality factor is used here to evaluate the selection performance. As for an example the quality factor is evaluated over a shower size and zenith angle bins by varying s_{local} which is shown in Table I. In Table II, we have given a chart for quality factors estimated at optimal conditions in three different situations.

A better option to evaluate the performance of selection algorithm is the application of an advanced technique like Principal Component Analysis or a Fisher analysis that allows to combine s_{local} and shower size in a single optimized observable.

7. Summary and conclusions

In this work, attempts have been made to discriminate γ-ray induced EAS from hadron initiated shower on the basis of shape of electron density distribution in EAS characterized by lateral shower age parameter that essentially reflects the stage of EAS development in atmosphere. Generally muon content of an EAS is treated as a good estimator for gamma-hadron discrimination. However, a precise measurement of total muons in an EAS requires muon detectors covering large area which is quite expensive. So, we explored whether lateral shower age could be used for the purpose.

We first explored traditional lateral shower age parameter i.e. single (r-independent) shower age as the distinguishing parameter. Later, we attempted to separate out γ-ray initiated EAS on the basis of mean LAP. It is found from the simulation results that γ-ray induced EASs are younger in terms of the mean LAP (i.e. having lower mean LAP) and hence this parameter (mean LAP) can effectively separate out γ-ray induced showers from hadronic EAS unlike the case of single lateral shower age. This is probably because of the inadequacy of a single (constant) lateral age parameter to describe the experimental lateral distribution of EAS electrons properly at all distances as noted in several experimental observations. So when a single constant age is assigned (from fitting of the electron density data at different radial distances) to an EAS event, the discriminating power of that parameter on primary masses somewhat becomes dull; it still can distinguish iron initiated showers from proton induced showers but can't effectively separate out γ-ray showers from EASs generated by primary protons. Fig. 2a is an indicative one in favor of the inadequacy of $s_\perp$ for gamma-hadron discrimination. It is clear from the figure that the $< s_\perp >$ values for γ-ray and proton induced showers are very much nearer to each other.

Lateral distribution of electrons in EAS exhibits universal (primary energy and mass independent) behavior in terms of LAP [40]. The present conclusion appears independent on the choice of high energy interaction models, or at least does not have strong interaction model dependence as both the QGSJet and EPOS give similar results.

An important question is the experimental realization of the adopted technique involving LAP. The uncertainty in estimating LAP is usually large in normal circumstances in comparison to that in lateral shower age as the LAP depends on the logarithmic derivative of the density versus radial distance. Thus, uncertainty in estimating LAP from experimental data arises mainly from the uncertainties in electron densities and those in radial distance measurements due to erroneous determination of shower core position. These uncertainties should be small for a closely packed air shower array like GRAPES-III at Ooty [44] or for a full coverage EAS array like ARGO-YBJ [25] and hence the proposed method may successfully work in a such kind of experiment. However, at present, the ARGO-YBJ carpet provides a full coverage area of about (80 m×80 m). For successful implementation of the proposed method, a slightly larger coverage area of the carpet would be desirable.

We also tried to identify γ-ray generated EAS by the use of 'f' parameter that describes the ratio of reconstructed average LEDs at two arbitrary distance bands from the shower core as proposed in [25,45]. It is found from the scatter plot of 'f '(as y variable) with the ratio of total muon content to total electron number (x variable) that EAS events are classified according to their respective primaries but the separation occurs not along y-axis rather along x-axis. This means that essentially the separation is due to the total muon content in EAS, a well studied mass sensitive observable.

Acknowledgments

The authors thank an anonymous referee for constructive comments and suggestions on our original manuscript. We are thankful to Prof. J. N. Capdevielle for many useful suggestions. R.K.D. thanks the UGC (Govt. of India) for support under Grant. No. 41/1407/2012(SR). R.K.D. thanks the USIC (NBU) for providing computational facilities.

References

[1] F. Aharonian et al., H.E.S.S. Collaboration, Astron. Astrophys. 457 (2006) 889.
[2] C. Baixeras, Nucl. Phys. B Proc. Suppl. 114 (2003) 247–252;
C. Baixeras, MAGIC Collaboration, Nucl. Phys. B Proc. Suppl. 175 (2008) 395.
[3] J.A. Hinton, New Astron. Rev. 48 (2004) 331.
[4] T.C. Weeks, The VERITAS Collaboration, 2010. <arXiv:1001.5305[astro-ph]>.;
M. Beilicke, VERITAS Collaboration, in: AIP Conference Proceedings, vol. 1112, 2008, pp. 33.
[5] W.B. Atwood et al., ApJ 697 (2009) 1071. <www-glast.stanford.edu>;
Charles D. Dermer. <arXiv:1206.2899[astro-ph.HE]>.
[6] W. Collmar et al., Astron. Astrophys. 354 (2000) 513–521.

[7] D.J. Bird et al., Fly's Eye collaboration, Phys. Rev. Lett. 71 (1993) 3401.
[8] R.U. Abbasi et al., HIRES collaboration, ApJ 622 (2005) 910.
[9] T. Antoni et al., Astropart. Phys. 24 (2005) 1–25.
[10] J. Abraham et al., Nucl. Instrum. Methods A 50 (2004) 523.
[11] F. Halzen, Pionic photons and neutrinos from cosmic ray accelerators, Astropart. Phys. (2011).
[12] T. Gaisser, Cosmic Rays and Particle Phys, Cambridge University Press, Oxford, 1990.
[13] S. Nestnhoff et al., Astropart. Phys. 4 (1995) 119–132.
[14] H.M. Badran, T.C. Neekes, Astropart. Phys. 7 (1997) 307–314.
[15] A. Bhadra, R.K. Dey, Mon. Not. Roy. Astron. Soc. 395 (2009) 1371–1375.
[16] P.R. Blake, W.F. Nash, J. Phys. G: Nucl. Part. Phys. 26 (2000) 365–375.
[17] A.W. Wolfendale, Nucl. Phys. B Proc. Suppl. 22 (1990) 80.
[18] J. Wdowczyk, A.W. Wolfendale, Nature 305 (1983) 609.
[19] M. Samorski, W. Stamm, ApJ Lett. 268 (1983) L17;
R.J. Protheroe, R.W. Clay, P.R. Gerhardy, ApJ Lett. 280 (1984) L47.
[20] K. Greisen, Progress in Cosmic Ray Physics, NH Publishing Co, Amsterdam, 1956 (vol. III);
H.S. Snyder, Phys. Rev. 76 (1989) 1563.
[21] J. Fenyves Techniques in UHE γ-ray astronomy, R.J. Protheroe, S.A. Stephens (ed.), (University of Adelaide, 1985) pp. 124; A.M. Hillas, in: Proc. 20th Int. Cosmic Ray Conference Moscow, vol. 2, 1987, pp. 362.
[22] D. Heck, et al., FZKA-Report Forschungszentrum Karlshruhe, 1998, pp. 6019.
[23] G. Disciascio et al., Int. J. Mod. Phys. A 20 (29) (2005) 6805–6807.
[24] J.N. Capdevielle, J. Gawin, J. Phys. G: Nucl. Phys. 8 (1982) 1317;
M.F. Bourdeau, J.N. Capdevielle, J. Procureur, J. Phys. G: Nucl. Phys. 6 (1980) 901;
J.N. Capdevielle, P. Gabinski, J. Phys. G: Nucl. Part. Phys. 16 (1990) 769.
[25] G. Disciascio, T.Di Girolamo, Astrophys. Space Sci. 309 (2007) 537–540;
A. Aloisio et al., Nuovo Cimento C24 (2001) 739.
[26] M. Nagano et al., J. Phys. Soc. Japan 53 (1984) 1667;
M. Nagano et al., J. Phys. G 10 (1984) 1295–1310.
[27] S. Sanyal et al., Aust. J. Phys. 46 (1993) 589.
[28] T. Antoni et al., Astropart. Phys. 14 (2001) 245.
[29] A. Bhadra et al., Nucl. Instrum. Methods A 414 (1998) 233.
[30] N.N. Kalmykov, S.S. Ostapchenko, A.I. Pavlov, Nucl. Phys. B (Proc. Suppl.) 5 (1997) 17.
[31] K. Werner et al., Phys. Rev. C 74 (2006) 044902.
[32] P. Lipari, Phys. Rev. D 79 (2009) 063001.
[33] A.A. Lagutin et al., in: Proc. 16th Int. Cosmic Ray Conf. Kyoto, vol. 7, 1979, p. 18
[34] J.N. Capdevielle et al., J. Phys. G: Nucl. Part. Phys. 31 (2005) 507–524.
[35] S. Tonwar, in: Proc. 17th Int. Cosmic Ray Conf., Paris, vol. 13, 1981, p. 330.;
M.V. Rao, in: Proc. 18th Int. Cosmic Ray Conf., Bangalore, vol. 11, 1983.
[36] H. Fesefeldt, Report PITHA-85/02 (RWTH Aachen) 1985.
[37] D. Heck, J. Knapp, J.N. Capdevielle, G. Schatz, T. Thouw, The CORSIKA air shower simulation program, Forschungszentrum Karlsruhe Report FZK 6019 (Karlsruhe), 1998.;
J.N. Capdevielle, The Karlsruhe Extensive Air Shower Simulation Code CORSIKA KfK Report 4998 (Karlsruhe), 1992.
[38] W.R. Nelson, H. Hiramaya, D.W.O. Rogers, Report SLAC, 1985, p. 265
[39] National Aeronautics and Space Administration (NASA) U.S. Standard Atmosphere Tech. Rep. NASA-TM-X-74335, 1976.;
J. Knapp, D. Heck Tech. Rep. 5196B Kernforschungszentrum Karlsruhe, 1993.
[40] R.K. Dey et al., J. Phys. G: Nucl. Part. Phys. 39 (2012) 085201.
[41] H. Ulrich et al., Nucl. Phys. B 175 (2008) 273;
H. Ulrich et al., Nucl. Phys. B 196 (2009) 80.
[42] W.D. Apel et al., Astropart. Phys. 24 (2006) 467.
[43] A. Bhadra, Pramana: J. Phys. 52 (1999) 133–144.
[44] S.K. Gupta et al., Nucl. Instrum. Methods A 540 (2005) 311.
[45] T.K. Gaisser, T. Stanev, Phys. Rev. D 43 (1991) 2.

IOP PUBLISHING JOURNAL OF PHYSICS G: NUCLEAR AND PARTICLE PHYSICS

J. Phys. G: Nucl. Part. Phys. **39** (2012) 085201 (14pp) doi:10.1088/0954-3899/39/8/085201

Scaling behaviour of lateral distribution of electrons in EAS

R K Dey[1], **A Bhadra**[2] **and J N Capdevielle**[3]

[1] Department of Physics, University of North Bengal, Siliguri, WB 734013, India
[2] High Energy and Cosmic Ray Research Centre, University of North Bengal, Siliguri, WB 734013, India
[3] APC, University Paris-Diderot, Bt. Condorcet, 10 rue Alice Domon et Leonie Duquet 75205 Paris Cedex 13 et Académie des Sciences d'Outre mer, 15 rue La Pérouse, 75116, Paris

E-mail: rkdey2007phy@rediffmail.com, aru-bhadra@yahoo.com and capdev@apc.univ-paris7.fr

Received 8 July 2011
Published 4 July 2012
Online at stacks.iop.org/JPhysG/39/085201

Abstract

From a Monte Carlo simulation study of cosmic ray air showers around the knee of the primary energy spectrum it is shown that, despite a strong radial dependence of the lateral shower age parameter, the lateral density distribution of electrons in cosmic ray EAS displays *universality* when expressed in terms of local age parameters. The nature of the radial variation of local age is found to depend on the choice of the effective Moliere radius, particularly for radial distances below about 400 m. The possible use of shower age parameters in a multi-parameter study of EAS for extracting information about the nature of the shower initiating particles, has been re-examined.

(Some figures may appear in colour only in the online journal)

1. Introduction

A number of recent studies indicate that the average shape of several distributions of electrons in very high energy cosmic ray extensive air showers (EAS), such as the energy distribution or angular distribution, primarily exhibits the so called *universality* [1–4]: it depends only on the stage of the longitudinal shower development in the atmosphere or equivalently on the longitudinal shower age parameters ($s_{||}$) (that represents the variation of the total number of EAS electrons with the atmospheric depth and hence describes the longitudinal shower development; details about the parameters are given in the next section) irrespective of the nature of the primary particle and energy. Such a feature was first divulged from the early work by Kamata and Nishimura [5] in the context of the development of cosmic ray cascades in the atmosphere. The experimental data also appear to substantiate this *universality* behaviour on an average basis [6]. The *universality* property is quite advantageous for the analysis of high energy cosmic ray data as it helps to parameterize the electron positron distributions, it seems useful for an accurate estimation of the muon and electromagnetic (EM) contents in an EAS

[7] and also it assists to infer the primary mass composition and the nature of the first few interactions from the observed EAS data [6].

The observed lateral density distribution (LDD) of EAS electrons is, however, usually described in terms of the lateral shower age ($s_\perp$), which essentially describes its slope. Theoretically, the relation $s_{||} = s_\perp$ holds for both EM showers and hadron initiated EAS [2, 5]. In most experiments, however, the estimated $s_\perp$ differs from $s_{||}$ for an EAS with hadrons as primary. Here note that $s_{||}$ can be estimated observationally only if the EAS experiment is equipped with Cherenkov or fluorescence detectors, whereas s_- follows immediately from the lateral distribution of electrons, which is a basic measurement of any conventional EAS array consisting of particle detectors. Hence it is imperative to explore the *universality* of LDD of EAS electrons in terms of the lateral shower age.

A major challenge, however, is the reliable and unambiguous estimate of $s_\perp$ from experimentally measured electron densities. Usually the LDD of electrons in an EAS is approximated by the well known Nishimura–Kamata–Greisen (NKG) structure function [8] and the shower parameters, namely the shower size (N_e) (the total number of electrons in an EAS at an observational level) and $s_\perp$ are evaluated by fitting the measured densities with the NKG function. However, experimentally it is observed that the NKG function with a single $s_\perp$ is insufficient to describe the LDD of EAS electrons properly at all distances, which implies that the lateral age changes with the radial distance. Subsequently some modifications of the NKG structure function [9] were proposed but the radial dependency on the shower age could not be removed totally. Under the circumstances, the notion of *local shower age parameters* (LAP) was introduced [10] which is in essence the lateral age at a point.

In this work, from a detailed Monte Carlo (MC) simulation study, we show that the shape of the radial variation of the LAP (and hence the LDD of the electrons in an EAS) exhibits some sort of *scaling* (energy and mass independent) behaviour. The shape of the radial variation of the LAP is, however, found to depend on the choice of the effective Moliére radius in the NKG function. Such a scaling feature provides a better description of the radial electron distributions in EAS and should help to estimate the electron content in an EAS accurately. We also investigate the characteristics of the LAP and its correlation with other EAS observables and thereby the possible role that the parameters may play in a multi-parameter approach to studying EAS, in order to understand the nature of shower initiating particles.

The plan of this paper is the following. In the next section the shower age parameters of EAS will be introduced. In section 3 the simulation procedure adapted in this work will be described. The estimation of the shower age parameters is given in section 4. The results on the characteristics of the local shower age and its correlation with other EAS observables will be given in section 5. Finally we will conclude in Section 6.

2. Shower age parameters

The average longitudinal profile of an EM cascade, which is developed in a medium through a multiplicative process involving the interactions of electrons and photons when passing through it, was provided by Greisen [8] in the so-called Approximation B (i.e., considering the processes like a pair production by the photons, *bremsstrahlung* by the electrons and the ionization loss suffered by the electrons while neglecting the Compton scattering)

$$N_e = \frac{0.31}{\sqrt{\ln(E_0/\epsilon_0)}} \exp[t(1 - 1.5\ln(s_{||})]. \tag{1}$$

Here E_0 is the energy of the primary photon generating the cascade, ϵ_0 is the critical energy (below which ionization losses predominate over that due to pair production) with a value

of ~82 MeV. Note that t is expressed here in cascade units (the atmospheric depth has been divided by the electron radiation length in air, taken as 37.1 gmcm^{-2}). The longitudinal age $s_{||}$ is defined by the simple relation

$$s_{||} = \frac{3t}{t + 2\ln(E_0/\epsilon_0)} . \tag{2}$$

The developmental stage of a pure EM cascade is thus characterized solely by $s_{||}$. Basically this parameter represents the change of the total number of EAS electrons with the atmospheric depth (dN/dt) [11]. Recent MC simulation studies [3, 4] exhibited a possible universality for large EAS with primaries in the EeV energy range in terms of $s_{||}$.

Advancing the preliminary work of Moliére and Bethe on the LDD of an electron near the cascade maximum, Nishimura and Kamata obtained an expression of radial distance dependence of $s_{||}$ by solving the three dimensional diffusion equations in Approximation B and taking into account the hegemony of the multiple Coulomb scattering [5]

$$s_{||}(r) = \frac{3t}{t + 2\ln(E/\epsilon_0) + 2\ln(r/r_m)} \tag{3}$$

where r is the radial distance from the shower core and r_m is the Moliére radius (near 80 m at sea level) which is a characteristic constant of a medium defined as the radius of a cylinder containing on average 90% of the EMS's energy deposition.

In the same theoretical context, the LDD of cascade particles can be approximated by the NKG structure function [8], given by

$$f(r) = C(s_\perp)(r/r_m)^{s_\perp - 2}(1 + r/r_m)^{s_\perp - 4.5} , \tag{4}$$

where the normalization factor $C(s_\perp)$ is given by

$$C(s_\perp) = \frac{\Gamma(4.5 - s_\perp)}{2\pi\Gamma(s_\perp)\Gamma(4.5 - 2s_\perp)} . \tag{5}$$

The NKG formula has the advantage of normalization as it is integrable in the Euler Beta function provided $s_\perp$ is independent of r. The normalization of $f(r)$ implies that $\rho(r) = N_e f(r)$, $\rho(r)$ being the electron density at r. The relation $s_{||} = s$ was considered to hold for pure EMS [5]. The equations (1), (2) and (4) together provide an attractive and a complete procedure for calculating the 3D development of the EM cascade, as first pointed out by Cocconi [12].

The superposition of many such pure EM cascades build the electron component of a hadron initiated EAS. It was suggested [2, 5] that for hadron initiated EAS, both the longitudinal structure and lateral structure of soft components can be described by that of a resulting single cascade, assigning a suitable value to the age parameter.

The various approximations made in obtaining the solutions, as well as due to an over-simplification of the adopted 3D transport equations, the analytical expressions of EM cascades are of restricted applicability. It was observed that near the shower axis, the NKG predicted densities were somewhat lower than those with the original NK formula [13] for $s \geqslant 1.2$. On the other hand, experimentally observed densities were noted to be larger than those given by the NKG far from the axis [8], which was inferred as a possible contribution from the muon decay. A shorter value of the second momentum of the distribution than in the NKG was observed [14] and a couple of years later a steeper profile was exhibited from an MC calculation near 100 GeV [15]. An improvement of the NKG function was subsequently proposed by adopting a modulated, longitudinal age parameter $s_{||}$ dependent effective Moliére

radius so that

$$\rho_{el}(r) = (mr_m)^{-2}\rho_{\mathrm{NKG}}(r/m) \tag{6}$$

where $m = 0.78 - -0.21s_{||}$.[4]

On the other hand, observing that the experimental LDD of electrons in EAS was steeper than that given by the ρ_{NKG} and was in better agreement with the MC calculations of Hillas [15] at lower energies, Capdevielle *et al* [10] introduced the notion of *local age*. After testifying the behaviour of the LAP on experimental lateral distributions [10] and reaffirming it with the Akeno observations [16], this approach was validated by the *rapporteurs* of the International Cosmic Ray Conferences during the period 1981 to 1985 [17]. The whole procedure was also employed in the calculation of the radio effects of EAS [18].

If electron densities are describing any NKG-like distribution $f(x)$, where $x = \frac{r}{r_m}$, for two neighbouring points, i and j, we have the (local) lateral age

$$s_{ij}^{\mathrm{local}} = \frac{\ln\left(F_{ij}X_{ij}^2Y_{ij}^{4.5}\right)}{\ln(X_{ij}Y_{ij})} \tag{7}$$

where $F_{ij} = f(r_i)/f(r_j)$, $X_{ij} = r_i/r_j$ and $Y_{ij} = (x_i{+}1)/(x_j{+}1)$. More generally, if $r_i \to r_j$, this suggests the definition of the LAP $s_{\perp}^{\mathrm{local}}(r)$ at each point:

$$s_{\perp}^{\mathrm{local}}(r) = \frac{1}{2x+1}\left((x+1)\frac{\partial \ln f}{\partial \ln x} + (2+\beta_0)x + 2\right) \tag{8}$$

If $\beta_0 = 4.5$, $f_{\mathrm{NKG}}(r)$ with $s_{\perp} \equiv s_{\perp}^{\mathrm{local}}(r)$ can be used to fit f in the neighbourhood of r.

Typical behaviour was predicted with a characterized minimum value of $s^{\mathrm{local}}(r)$ near 50 m from the axis, followed by a general increase at a large distance [10]. The relation $s_{\perp}^{\mathrm{local}}(r) = s_{ij}^{\mathrm{local}}$ for $r = \frac{r_i+r_j}{2}$ was found to be valid for the experimental distributions (taking $F_{ij} = \rho(r_i)/\rho(r_j)$ as far as they were approximated by monotonic decreasing functions versus distance).

Such a prediction was substantiated by the Akeno [16], North Bengal University (NBU) EAS experiment [19] and other experiments [10]. The LAP depends mainly on the logarithmic derivative of the density versus the distance as it appears in the relation (9); however, this pure mathematical approach may not be attained in practice at any radial distance, due to the experimental uncertainties arising mainly from the use of a finite number of detectors for the density measurements, triggering conditions and errors in the determination of the shower core position. Therefore, $s_{\perp}^{\mathrm{local}}(r)$ is estimated via relation (7) using physical bands of distance $[r_i, r_j]$; for experiments with very dense grids of detectors, such distance bands may be reduced to 5–10 m, but they may have to enlarge up to about 20 m for arrays with a lower resolution, as well as in the case of individual showers with large fluctuations. For very large and giant EAS, the interval $[r_i, r_j]$ maybe required to exceed 100 m or so. We preferred to conserve the characteristic parameters of EM cascades in relation (7) including the value of the Moliére radius to facilitate the comparison with the experimental data, which is most frequently expressed in NKG formalism.

The dependence of $s_{\perp}(r)$ on r rules out a consistent integration via relation (4) casting some doubt on the accurate relation between density and size; it was shown that such a dependence of $s_{\perp}(r)$ on r is mainly a basic feature of pure EM cascades [10, 20].

[4] ρ_{el}, not just ρ_{NKG}, was implemented in the so called subroutine NKG of CORSIKA (Cosmic Ray Simulation for KAscade).

3. Method of simulation

For generating EAS events, the air shower simulation program CORSIKA [21] is exploited here. Here our discussions are mainly restricted to cosmic rays in the knee region of the primary spectrum. In this work, the high energy (above 80 GeV/n) hadronic interaction model QGSJET 01 version 1c [22] was used in combination with the low energy (below 80 GeV/n) hadronic interaction model GHEISHA (version 2002d) [23] or FLUKA [24], depending on the primary energy in the framework of the CORSIKA MC program version 6.600/6.735 [21] to generate EAS events. Note that the low energy interaction model GHEISHA exhibits a few shortcomings [25, 26] but the LDD of EAS electrons does not depend much on the low energy hadronic models, except at large distances [25]. Hence for very high energy events involving large radial distances we employed FLUKA [24]. A relatively smaller sample was also generated using the high-energy interaction model SIBYLL (version 2.1) [27] to judge the influence of the hadronic interaction models on the results.

The CORSIKA program allows one to choose either of the two options, the EGS4 (electron gamma shower system version 4) [28] and the NKG for obtaining a lateral distribution of the charge particles. The former option facilitates a detailed MC simulation of the EM component of a shower that incorporates all the major interactions of electrons and photons (see [11]), whereas the NKG option relies on an analytical approach rather than a full MC simulation. In the NKG option, the electron density of an EM sub-shower is calculated straightaway using the NKG function with a reduced Moliére radius [9, 10]. One gets better accuracy and more detailed information about the EM component with the EGS4 option, at the expense of long computing time. We underline here that the NKG option (subroutine NKG inside CORSIKA)[5] is dealing mainly with the relations ((6), (7)) and not directly with equation (4).

We have considered the US-standard atmospheric model [31] with a planar approximation. The maximum primary zenith angle was restricted to 50°. The EAS events were generated mainly for proton and iron nuclei as primaries. A few events were also generated for γ as primary. Irrespective of the nature of the primaries, the slope of primary power law spectra was taken as -2.7 below the knee (3×10^{15} eV) and as -3.0 above. The EAS events were simulated at different geographical positions corresponding to the experimental sites of AKENO [16], KASCADE [30] and NBU [32]. The magnetic fields are provided accordingly. On the observational level, the kinetic energy thresholds were chosen as 3 MeV for electrons (e^+ and e^-) irrespective of the primary species and energies.

3.1. Generation of the EAS Monte Carlo library

The simulated shower library consists of more than 30 000 EAS events with the EGS4 option and more than 180 000 events with the NKG option in the primary energy interval of 10^{14} eV to 3×10^{16} eV. In order to appreciate the asymptotic tendencies at ultra high energies, our library has also been enriched by about 1000 events simulated at $E_o = 5 \times 10^{17}$ and 10^{18} eV for proton and iron primaries: apart from the thinning factor which is taken as 10^{-6} with optimum weight limitation [33] (i.e., all particles are followed up to an energy $E_{\rm th}$, where $E_{\rm th}/E_o = 10^{-6}$, after which only one of those particles is tracked giving appropriate weight to it) the simulation conditions are here identical concerning the hadronic interaction models, the zenith angle range, both the EGS4 and the NKG options. Here we would like to specify that the optimized thinning factor 10^{-6} with the optimum weight limitation for the CORSIKA

[5] Reference [29] in the original documentation of CORSIKA was mismatched with the appropriate references [10]; it was unfortunately reproduced in the user's guide and in several papers, as for instance [30], thereby generating a confused interpretation of the NKG option.

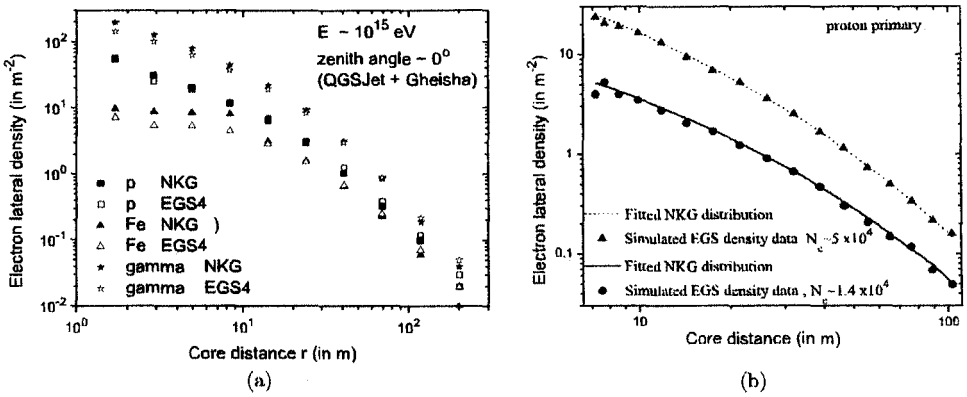

Figure 1. Lateral distribution of electrons from the simulated data. (a) Comparison of the EGS4 and the NKG output for different primary cosmic ray species, (b) NKG fitting of the EGS4 output of electron density at the NBU site with a constant single age restricting radial distance only up to 100 m. The statistical errors are within the dimensions of the symbols used.

version used here is considered as the best compromise between the computing time and the accuracy at ultra high energies [34].

In all cases involving the EGS4 option, the longitudinal development is restored numerically and that $s_{||}$ is computed [35], instead of relation (2), by:

$$s = \exp\left[\frac{2}{3} \times \left\{1 + \frac{\alpha}{t} - \tau\right\}\right] \quad \text{with } \tau = \frac{t_{\max}}{t}, \ \alpha = \ln\frac{N_{\max}}{N_e} \tag{9}$$

where $t_{\max}$, $N_{\max}$ are respectively depth and size read at the cascade maximum.

3.2. The NKG and the EGS options

We used both the EGS4 and the NKG options simultaneously for about 30 000 events. In figure 1(a) we compare the LDD of EAS electrons obtained with the stated two options for proton, iron and gamma primaries. It is noted that the NKG option gives a higher density with a steeper radial distribution compared to the EGS option. A small density excess appears for the pure EM cascades near the axis for the NKG option; such an excess presents also in the proton initiated air showers. However, for the proton showers, a tolerable agreement between the output of the two options was noted over a large band of densities between radial distances of 10–100 m from the shower axis; it reconfirms that for proton and photon initiated showers the NKG option is quite useful to calculate a large number of cascades in a short time.

For Fe primaries, both the options indicate an older profile near the axis. The NKG option was found to give an excess density between 2–10 m distance. The average energy of the positrons was quite a bit lower in the case of iron initiated showers and the cross section of positron annihilation becomes more important for the lower part of the cascade. This effect is probably enhanced by the longer path of the electrons in the geomagnetic field and the larger energy loss by ionization. The NKG option is, therefore, not so accurate for the simulation of heavy nuclei initiated showers with large zenith angles after the shower maximum. For vertical showers, the output of the NKG option is nevertheless acceptable. At larger distances a slight deficit in the densities appears with the NKG option; this probably comes from the different treatment of the multiple Coulomb scattering in the NKG option than in the EGS. Furthermore, Bhaba and Moller scattering are treated in complement with the separated MC

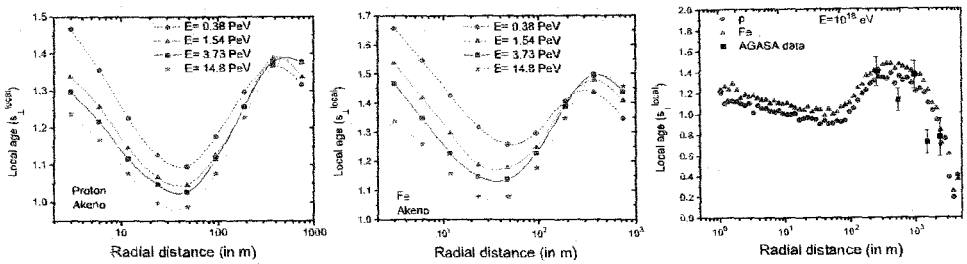

Figure 2. Variation of the LAP (estimated from the simulated data) with radial distance for different primary energies at AKENO site (920 g cm^{-2}) for (a) p (b) Fe (c) for both p and Fe along with the local age obtained from the experimental data. The lines are only a guide for the eye.

procedures. On the other hand, the geomagnetic field of the earth enhances the path of the muons. Consequently their loss by ionization and their decay give more electrons, which is not incorporated in the NKG option. Besides, the NKG option does not accommodate photo-production inside the EM sub-cascades.

4. Estimation of shower age

The simulated data were analysed using the reconstruction algorithms developed to obtain shower size and shower age. We adopted two different methods. First following the traditional approach, we estimated the basic shower parameters by fitting the density data to the NKG function by the method of chi-square minimization through an iterative procedure based on the method of steepest decent. As for example, in figure 1(b) the simulated particle densities at different radial distances are plotted along with the fitted curve obtained with the NKG function. Here it is noted that the majority of the EAS groups traditionally estimate basic shower parameters based on the NKG function. The error in estimating lateral shower age in the shower size interval 10^3–10^5 particles (corresponding to the primary energy range 10^{14}–3×10^{15} eV) was found to be ± 0.03 for the QGSJET model and ± 0.05 for the SIBYLL. The larger error for the SIBYLL model seems solely statistical, due to the generation of a relatively fewer number of EAS events using the later model.

The local age for EAS charged particles was computed for each individual event straightaway, applying equation (7). When estimating the LAP, the main sources of error are the fluctuations in particle density and the uncertainties in radial distance estimation. In simulated data the radial distance of each particle is known with a high accuracy. In this work the error in the LAP, due to uncertainties in radial distance estimation, was kept small by taking small radial bins. For minimizing the statistical fluctuations in particle density at different radial bins, a large number of events need to be considered. In this analysis, the error of the LAP for EAS with the primary energy in the PeV range remains within 0.05 for 10 m $< r <$ 250 m, whereas for $r <$ 10 m or when $r >$ 300 m the error of the LAP is found to be higher, about 0.1. At higher primary energies (5×10^{17}–10^{18} eV) the error of the LAP is found at about 0.12 near the core, which decreases to about the 0.07 level when 20 m $< r <$ 300 m but increases again with the radial distance and reaches to about 0.15 when r approaches 1000 m.

The variation of the LAP with the radial distance from the shower core is shown in figure 2. It is known from previous studies [10] that with an increase of the radial distance, the

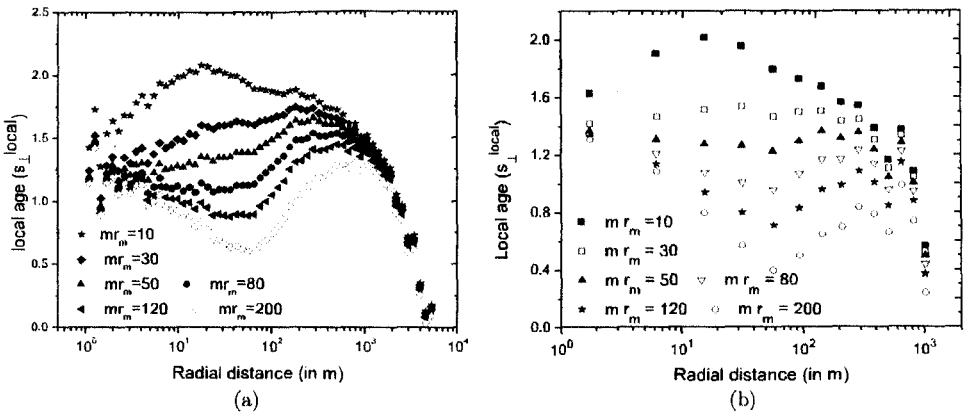

Figure 3. Variation of the LAP (estimated from the simulation data) with the radial distance for different choices of the effective Moliére radius at the KASCADE site (a) for p with a primary energy 5×10^{17} eV (b) for γ with a primary energy 10^{15} eV.

LAP initially decreases, reaching a minimum at around 50 m and then increases, as was also noted from the experimental data [16, 19,10]. Here we noticed two other interesting features (figure 2(a)–(c)): the local age again starts to decrease at around 300–400 m. To examine whether the experimental data also demonstrates a fall in the local age at large radial distances, we compute the local age from the LDD data of total charged particles, as measured by the AGASA experiment [36] for primary energy 2×10^{18} eV and compared these values with our simulation results in figure 2(c). The experimental data clearly support the trend predicted by the simulation results at larger radial distances. The characteristic high–low–high kind of radial variation in the local age at relatively smaller distances (within 300 m or so) could not be substantiated by the AGASA data, due to the large separation of the detectors of the array. It is worthwhile mentioning that there was an indication for such a decrease of $s_\perp^{local}(r)$ at around 300 m in the experimental results obtained by Akeno [19] and KASCADE-Grande [37]. Such behaviour is also depicted in figure 3 of the Kascade report [30], where one may notice a maximal deficit at 50–80 m in the ratio of the measured and the fitted electron densities, as well as an excess at large distances when fitting with the NKG formula. The later feature, however, has not been thoroughly investigated.

These findings are important for an analysis of very large air showers observed/to be observed by the KASCADE-Grande, AGASA, AUGER, Yakutsk, Telescope Array involving large radial distances. The large EAS experiments often treat charged particle densities at large radial distances, such as at 500, 600, 1000 m from the shower core as an estimator of the primary particle energy, though such a technique involves several uncertainties [38]. These findings, of a rapid change in the slope of the radial distribution of electrons at large radial distances, suggest that more controls should be adopted in the estimation of the primary energy of large showers, for instance by taking particle densities at more than one radial distance.

Another important observation is that in general the nature of the variation of the local age with the radial distance appears nearly the same for all of the primary energies, i.e. the nature of the variation is practically independent of the energy of the shower initiating particles, which implies that the local age (or the lateral distribution of electrons in EAS) exhibits some sort of scaling behaviour in respect to the radial dependence from the shower core.

To examine systematically the influence of the effective Moliére radius on the shape of the lateral distribution of charged particles in EAS, we study the radial variation of the LAP for different effective Moliére radii, which is shown in figure 3(a) for a proton primary with a primary energy 5×10^{17} eV.

A string-like feature emerged with two nodes, as seen from the figures, one close to the shower core while the other at around $r \sim 400$ m that increases slowly with the effective Moliére radius; the effective Moliére radius behaves somewhat like the tension in a piece of string. Beyond the second node, however, the LAP is found to decrease monotonically with an increase of the radial distance, irrespective of the choice of the effective Moliére radius.

In order to explore the inherent cause of such a feature of the LDD of electrons in hadron initiated EAS, we studied the radial variation of the local age for γ ray initiated showers, and one such plot at the primary energy 10^{15} eV is shown in figure 3(b). We found the similar nature of radial variation of the LAP as in the hadron initiated showers. As ascertained in previous simulations [10], the behaviour of $s^{\text{local}}(r)$ comes mainly from the discrepancies between the EGS output and the NKG function, i.e. between the rigorous descriptions of the EM cascade adopting the basic EM processes as well as the Moller, Bhabha scattering, positron annihilation, dependence of the cross section on energy on the one hand, Approximation B combined with Landau and small angle approximations in a single description of the multiple Coulomb scattering on the other hand. When the experimental data [30, 35] are superimposed on figure 3, we understand that a reduced Moliere radius (between 20–50 m) is favoured for all primary energies, implying a dramatic reduction in the mean scattering angle connected with the scattering energy of 21 MeV.

5. Characteristics of the shower age parameter

To explore the physical nature associated with the lateral shower parameter, if any, we studied the details of the characteristics of the shower age. For the local age, we considered two different parameters: the minimum value corresponds to the local age at the radial distance, about 40 m, and an average value between 40 to 300 m.

5.1. Distribution of shower age and its fluctuation

The distributions of the LAP and the lateral shower age were studied for the primary energy range 3×10^{14} to 3×10^{16} eV. The fluctuations in the shower age were found to be larger for proton initiated showers compared to those initiated by a heavier primary. If we consider a small primary energy bin instead of a wide one, for instance by selecting the showers inside a small muon size band, we observed that both the distributions of p and Fe could be separated, which in fact becomes very contrasted as shown in figure 4(a); this approach, if adopted with the experimental data, may yield important information on the primary composition around the knee region.

The fluctuations (σ) (variance) in the LAP in different shower age bins are estimated and as a function of the shower size are drawn in figure 4(b) for proton and iron primaries for the interaction model QGSJET. In accordance with expectations [39], the fluctuations in the LAP were found to be larger for the proton initiated showers in comparison to those initiated by the primary Fe, except at lower energies.

5.2. Longitudinal shower age versus lateral shower age

For each simulated event, the longitudinal shower age was also estimated using the relation (9) and the difference between the two age parameters, longitudinal age and average local age,

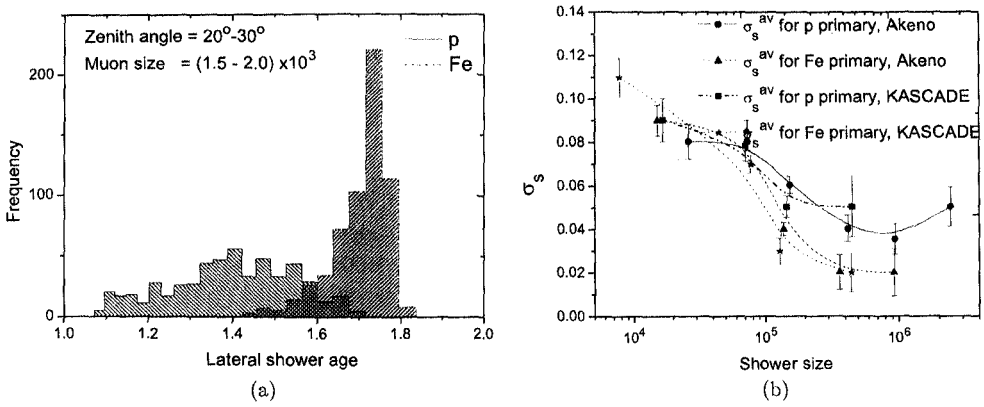

Figure 4. (a) Distribution of the lateral age parameter from simulation at sea level for p and Fe primaries within a small muon size window and (b) the variance (σ) of the distribution of the LAP as a function of shower size. The lines are only a guide for the eye.

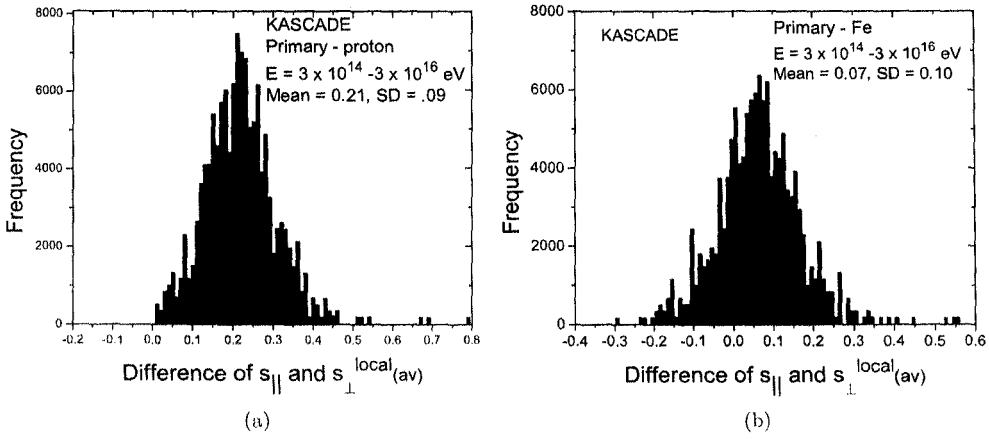

Figure 5. Distribution of the difference between the longitudinal shower age and local shower age from simulated data for (a) p and (b) iron primaries at the KASCADE location.

was obtained. The frequency distributions of the differences between the two age parameters for proton and Fe primaries are given in figure 5. The frequency distribution for where the proton primary peaks, at around 0.2, is consistent with the early observations [40, 10], whereas for Fe initiated showers the peak difference is much lower, at about 0.07. However, for a non-negligible fraction of events, the differences between the two shower age parameters were found to be substantial.

5.3. Variation of the shower age with electron size

In figure 6, we plot the local shower age at a radial distance of about 40 m (minimum value) versus an average shower size, obtained from the simulation results for both proton and iron primaries at the Akeno and KASCADE locations. The corresponding observational results

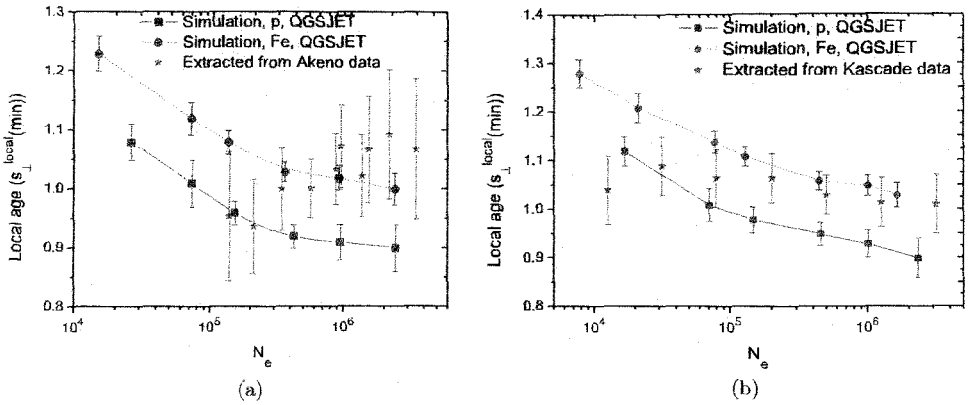

Figure 6. variation of the lateral shower age with shower size for proton and Fe primaries at the (a) Akeno and (b) KASCADE locations. The lines are only a guide for the eye.

extracted from the Akeno and KASCADE experimental data are also given in figure 6. For the Akeno experimental data, we extracted a minimum local age for the different shower sizes from reference [16], whereas for KASCADE we estimated it from their measured lateral distribution [30, 37,42].

The comparison of the simulated results with the experimental observations from both the Akeno and KASCADE EAS experiments (figure 6) indicate a need for a change in the primary composition towards a heavier primary, as the energy increases across the knee of the primary energy spectrum. The KASCADE group also reached a similar conclusion using the shape parameter instead of the shower age [42], as well as from the study of the muon content in EAS [43]. The present data of the LHC, especially the pseudo-rapidity density distributions, suggest larger multiplicities and inelasticities than in the models used in the CORSIKA simulations [44]. However, up to an energy of 2.6×10^7 GeV, this could result in a very small reduction of the reported enhancement of the primary mass with energy.

6. Conclusions

From the present analysis we conclude the following.

(1) The lateral distribution of electrons in EAS exhibits some sort of scaling (energy independent) behaviour in terms of the local age. The characteristic feature of the local age versus the radial distance curve is that with an increase of the radial distance, the local age decreases initially and reaches a minimum, at around 40 m, then it starts increasing, attaining a local maxima, at around 300–400 m, and then starts decreasing again. Such a feature appears to be independent of the energy of the EAS initiating particle, at least there is no strong dependence on the primary energy. Such a characteristic radial variation in the local age is found as a generic feature of EM cascades.

(2) The local age offers a good solution towards an unambiguous estimation of the shower age. Since the shower age varies with the radial distance, even for the modified NKG functions, a comparison of the lateral shower age of different EAS experiments is not meaningful, as the radii of the shower discs naturally differ from experiment to experiment, depending on the experimental set up. Even in a single EAS experiment different events have different

radial extensions and thus a lateral age obtained through fitting with the NKG function seems ambiguous. The local age at a particular distance (say at about 40 m where it takes the minimum value) is, however, not always practical owing to the large fluctuation in the electron density data in a real measurement. A rational idea could be to take some sort of average local age between the first minimum, at around a core distance of 40 m, and the subsequent local maximum, at around 300 m. Experimentally the radial variation of the LAP can be checked properly with a full coverage detector array, like the ARGO-YBJ [45].

(3) The use of a reduced effective Moliére radius in the NKG function leads to a roughly constant age over a radial distance up to about 200 m [41], but the shower age estimated in such a manner is found take quite a higher value than that of the longitudinal age. More importantly, even with a reduced effective Moliére radius, the local age is still found to vary after a radial distance of about 200 m.

(4) The lateral age offers a good estimator of the longitudinal development of an EAS cascade, as already noted in some earlier works [46, 40,10]. However, the parameter correlates with the stage of the shower development on a statistical basis; the average of this parameter increases as air showers traverse an increased thickness of atmosphere. The experimental observations [20] also substantiate such behaviour. The distribution of the differences between the local age and the longitudinal age also indicate the strong correlation between the two ages. Such a feature has been noted for two different hadronic interaction models, the QGSJET and the SIBYLL, and hence appears robust. It is imperative to examine such correlations using EPOS [47], the only model that seems to be providing quite a consistent description of the longitudinal and lateral EAS profiles [48], which would need to be performed in future work.

(5) The fluctuation of the LAP was found to be sensitive to the nature of the primary particle. However, the level of uncertainty in determining the lateral shower age from the experimental data is comparable with the magnitude of fluctuation and hence deriving any firm conclusion on the nature of the primary only from the shower age fluctuation is difficult. If showers within a small bin of the primary energy could be selected, for instance by considering shower events in a small muon size interval, the distribution of shower age was found to be quite sensitive on primary composition; this property may be useful (in conjunction with other primary sensitive parameters) to extract information about primaries.

The comparison of the simulation results with the Akeno and the KASCADE observations in respect to a variation of the shower age with shower size around the knee indicates a change in the primary composition towards heavier primaries across the knee. This finding supports the results obtained from the study of the muon content in EAS. The 3D plot of the shower size versus muon size and shower age may improve accuracy over the conventional approach: deducing the composition through the shower size versus muon size curve. It would be an interesting task to apply such a method for a composition study using observed EAS data from a closely packed air shower array with the facility of concurrent muon measurements, such as the GRAPES experiment at Ooty [49].

Acknowledgments

The authors sincerely thank two anonymous referees and a board member for critical comments and helpful suggestions. AB would like to thank the Department of Science and Technology (Govt. of India) for support under the grant no. SR/S2/HEP-14/2007.

References

[1] Giller M, Kacperczyk A, Malinowski J, Tkaczyk W and Wieczorek G 2005 *J. Phys. G: Nucl. Part. Phys.* **31** 947
Nerling F, Blumer J, Engel R and Risse M 2006 *Astropart. Phys.* **24** 421
[2] Lipari P 2009 *Phys. Rev.* D **79** 063001
[3] Lafebre S, Engel R, Falcke H, Hörandel J, Huege T, Kuijpers J and Ulrich R 2009 *Astropart. Phys.* **31** 243
[4] Schmidt F, Ave M, Cazon L and Chou A 2008 *Astropart. Phys.* **29** 355
Gora D *et al* 2006 *Astropart. Phys.* **24** 484
[5] Kamata K and Nishimura J 1958 *Prog. Theor. Phys. Suppl.* **6** 93
[6] Yushkov A *et al* 2010 *Phys. Rev.* D **81** 123004
[7] Apel W D *et al* 2008 *Astropart. Phys.* **29** 412
[8] Greisen K 1956 *Progress in Cosmic Ray Physics* vol III (Amsterdam: North Holland)
Greisen K 1960 *Annu. Rev. Nucl. Part. Sci.* **10** 63
Snyder H S 1989 *Phys. Rev.* **76** 1563
[9] Lagutin A A *et al* 1979 *Proc. 16th Int. Cosmic Ray Conf. (Kyoto)* vol 1 p 18
Uchaikin V V 1979 *Proc. 16th Int. Cosmic Ray Conf. (Kyoto)* vol 1 p 14
[10] Capdevielle J N and Gawin J 1982 *J. Phys. G: Nucl. Phys.* **8** 1317
Bourdeau M F, Capdevielle J N and Procureur J 1980 *J. Phys. G: Nucl. Phys.* **6** 901
Capdevielle J N and Gabinski P 1990 *J. Phys. G: Nucl. Part. Phys.* **16** 769
[11] Rossi B and Greisen K 1941 *Rev. Mod. Phys.* **13** 240
[12] Cocconi G 1961 *Handbuch der Physik: Cosmic Rays* I vol 46/1 (Berlin: Springer) p 215
[13] Nishimura J 1967 *Handbuch der Physik: Cosmic Rays* II vol 46/2 (Berlin: Springer) p 1
[14] Allan H R *et al* 1975 *Proc. 14th Int. Cosmic Ray Conf. (Munich)* vol 8 p 2131
[15] Hillas M and Lapikens J 1977 *Proc. 15th Int. Cosmic Ray Conf. (Plovdiv)* vol 8 p 460
[16] Nagano M *et al* 1984 *J. Phys. Soc. Japan* **53** 1667
[17] Tonwar S 1981 *Proc. 17th Int. Cosmic Ray Conf. (Paris)* vol 13 p 330
Rao M V S 1983 *Proc. 18th Int. Cosmic Ray Conf. (Bangalore)* vol 11 p 449
Clay R W 1985 *Proc. 19th Int. Cosmic Ray Conf. (La Jolla)* vol 9 p 323
[18] Suprun D, Gorham P W and Rosner J L 2003 *Astropart. Phys.* **20** 157
[19] Sanyal S *et al* 1993 *Aust. J. Phys.* **46** 589
[20] Bhadra A 1999 *Pramana J. Phys.* **52** 133
[21] Heck D, Knapp J, Capdevielle J N, Schatz G and Thouw T 1998 The CORSIKA air shower simulation program *Forschungszentrum Karlsruhe Report* FZK 6019 (Karlsruhe)
Capdevielle J N 1992 The Karlsruhe Extensive Air Shower Simulation Code CORSIKA *KfK Report* 4998 (Karlsruhe)
[22] Kalmykov N N, Ostapchenko S S and Pavlov A I *et al* 1997 *Nucl. Phys.* B **52** 17
[23] Fesefeldt H 1985 *Report PITHA-85/02* (RWTH Aachen)
[24] Fassò A *et al* 2001 *Proc. Monte Carlo 2000 Conf. (Lisbon)* (Berlin: Springer) p 955
[25] Drescher H J *et al* 2004 *Astropart. Phys.* **21** 87
[26] Bhadra A *et al* 2009 *Phys. Rev.* D **79** 114027
Heck D 2006 *Nucl. Phys.* B **151** 127
Ferrari A and Sala P R 1996 *ATLAS Int. Note PHYS-No-086* (Geneva: CERN)
[27] Fletcher R S, Gaisser T K, Lipari P and Stanev T 1994 *Phys. Rev.* D **50** 5710
[28] Nelson W R, Hirayama H and Rogers D W O 1985 The EGS4 Code System *Report* SLAC265 (Stanford Linear Accelerator Center, Stanford, CA)
[29] Capdevielle J N *et al* 1977 *Proc. 15th Int. Cosmic Ray Conf. (Plovdiv)* vol 8 p 341
[30] Antoni T *et al* 2001 *Astropart. Phys.* **14** 245
[31] National Aeronautics and Space Administration (NASA) 1976 US standard atmosphere *Technical Report* NASA-TM-X-74335
Knapp J and Heck D 1993 *KfK Technical Report* 5196B (Kernforschungszentrum Karlsruhe)
[32] Bhadra A *et al* 1998 *Nucl. Instrum. Methods* A **414** 233
[33] Kobal M 2001 *Astropart. Phys.* **15** 259
[34] Knapp J, Heck D, Sciutto S J, Dova M T and Risse M 2003 *Astropart. Phys.* **19** 77
[35] Capdevielle J N and Cohen F 2005 *J. Phys. G: Nucl. Part. Phys.* **31** 507
Capdevielle J N and Cohen F 2005 *J. Phys. G: Nucl. Part. Phys.* **31** 1413
[36] Yoshida S *et al* 1994 *J. Phys. G: Nucl. Part. Phys.* **20** 651
[37] Ulrich H *et al* 2008 *Nucl. Phys.* B **175** 273
Ulrich H *et al* 2009 *Nucl. Phys.* B **196** 80

[38] Capdevielle J N *et al* 2009 *J. Phys. G: Nucl. Part. Phys.* **36** 075203
[39] Catz Ph *et al* 1973 *Proc. of the 13th Int. Cosmic Ray Conf. (Denver, USA)* vol 4 p 2495
[40] Dedenko L G *et al* 1975 *Proc. 14th Int. Cosmic Ray Conf. (Munchen)* vol 8 p 2731
Stamenov J N 1987 *Proc. 20th Int. Cosmic Ray Conf. (Moscow)* vol 8 p 258
[41] Nagano M *et al* 1984 *J. Phys. G: Nucl. Part. Phys.* **10** 1295
[42] Apel W D *et al* 2006 *Astropart. Phys.* **24** 467
[43] Antoni T *et al* 2002 *Astropart. Phys.* **6** 245
[44] Capdevielle J N 2010 arXiv:1010.0916v1
[45] Aloisio A *et al* 2001 *Nuovo Cimento* C **24** 739
[46] Dixon H E and Turver K E 1974 *Proc. R. Soc. Lond.* A **339** 171
[47] Werner K, Liu F-M and Pierog T 2006 *Phys. Rev.* C **74** 044902
Pierog T and Werner K 2009 *Nucl. Phys.* B **196** 102
[48] Pierog T and Werner K 2008 *Phys. Rev. Lett.* **101** 171101
[49] Gupta S K *et al* 2005 *Nucl. Instrum. Methods* A **540** 311

Mon. Not. R. Astron. Soc. 395, 1371–1375 (2009) doi:10.1111/j.1365-2966.2008.14345.x

TeV neutrinos and gamma-rays from pulsars

A. Bhadra[1]★ and R. K. Dey[2]★

[1]*High Energy and Cosmic Ray Research Centre, University of North Bengal, Siliguri, WB 734013, India*
[2]*Department of Physics, University of North Bengal, Siliguri, WB 734013, India*

Accepted 2008 December 9. Received 2008 December 9; in original form 2008 September 27

ABSTRACT

Recent studies suggest that pulsars could be strong sources of TeV muon neutrinos provided positive ions are accelerated by pulsar polar caps to PeV energies. In such a situation, muon neutrinos are produced through the Δ-resonance in interactions of pulsar-accelerated ions with its thermal radiation field. High-energy gamma-rays should also be produced simultaneously in pulsar environment as both charged and neutral pions are generated in the interactions of energetic hadrons with the ambient photon fields. Here, we estimate TeV gamma-ray flux at the Earth from a few nearby young pulsars. When compared with the observations, we find that proper consideration of the effect of polar cap geometry in flux calculation is important. Incorporating such an effect, we obtain the (revised) event rates at the Earth due to a few potential nearby pulsars. The results suggest that pulsars are unlikely to be detected by the upcoming neutrino telescopes. We also estimate TeV gamma-ray and neutrino fluxes from pulsar nebulae for the adopted model of particle acceleration.

Key words: neutrinos – pulsars: general – gamma-rays: theory.

1 INTRODUCTION

Probable candidates of high-energy neutrino radiation include gamma-ray bursts, active galactic nuclei, etc. (Halzen & Hooper 2002). Recently, Link & Burgio (LB) (Link & Burgio 2005, 2006) have shown that pulsars could also be a strong source of high-energy neutrinos. As per their results, pulsars with a magnetic moment component antiparallel to the spin axis, which is expected in half of the total neutron stars, could emit TeV muon neutrinos with fluxes observable by the operating or planned large area neutrino observatories. As a conjecture to be verified by observations, LB considered that protons or heavier ions are accelerated near the surface of the pulsar by the polar caps to PeV energies. When these accelerated ions interact with the thermal radiation field of pulsar, the Δ-resonance state may occur provided their energies exceed the threshold energy for the process. Though radiation losses limit the maximum energy that can be attained by the nuclei in the acceleration process, such an energy condition is expected to satisfy for several pulsars. Muon neutrinos are subsequently produced from the decay of Δ-particles.

The presence of a hadronic component in the flux of pulsar-accelerated particles should result in the emission of high-energy neutrinos and gamma-rays simultaneously as both charged and neutral pions are produced in the interactions of energetic hadrons with the ambient photon fields surrounding the acceleration region. Here, we would show that for the model adopted by LB the estimated TeV gamma-ray fluxes from several nearby pulsars are higher than the observed upper limits of fluxes. In the quest for reasons of such inconsistency, we note that an implicit assumption in the LB estimation of neutrino flux is that the polar cap area is equal to the neutron star surface area. Such an assumption seems unreasonable in view of the polar cap geometry (Beskin, Gurevich & Istomin 1993). When this fact is taken into consideration, the stated inconsistency between the estimated and the observed gamma-ray fluxes is found to disappear. In view of this observation, the revised estimates of the neutrino fluxes from a few known gamma-ray pulsars are obtained by incorporating polar cap geometry.

A young neutron star is generally encircled by pulsar wind nebula (PWN). Positive ions, after gaining energy from polar gaps, will move away from the pulsar practically along the open field lines and will finally inject into the nebula. It is very likely that these energetic ions would be trapped by the magnetic field of the nebula for a long period, and consequently they should produce high-energy gamma-rays and neutrinos by interacting with the matter of the nebula. We therefore estimate the expected flux of TeV gamma-rays from pulsar nebulae, and by comparing with the observation for a couple of well-known nebulae we check the consistency of the model. We also calculate the flux of TeV neutrinos from a couple of pulsar nebulae.

This article is organized as follows. In the next section, after describing the generation of the TeV gamma-rays and neutrinos in a pulsar environment, the expected flux of gamma-rays from a pulsar is estimated for the polar cap model of acceleration as used by LB. By comparing the model-predicted gamma-ray fluxes from

★E-mail: aru_bhadra@yahoo.com (AB); rkdey2007@rediffmail.com (RKD)

some potential young pulsars with the observations, the importance of the inclusion of polar cap area in the calculation has been stressed in Section 3. Incorporating such a feature, (revised) event rates in a neutrino telescope at the Earth due to a few potential pulsars are obtained in Section 4. In Section 5, fluxes of TeV gamma-rays and neutrinos from pulsar nebulae are obtained for the adopted model, and finally the results are concluded in Section 6.

2 TEV GAMMA-RAYS AND NEUTRINOS FROM PULSARS

Several detailed mechanisms have so far been suggested for acceleration of particles by pulsars that include the popular polar gap (Ruderman & Sutherland 1975; Arons & Scharlemann 1979; Daugherty & Harding 1996; Harding & Muslimov 1998) and the outer-gap models (Cheng, Ho & Ruderman 1986). In the former model, acceleration of particles takes place in the open field line region above the magnetic pole of the neutron star whereas in the case of outer-gap model it occurs in the vacuum gaps between the neutral line and the last open line in the magnetosphere. Thus, the region of acceleration in the polar-gap model is close to the pulsar surface, while the same in the outer-gap model is close to the light cylinder.

In the polar cap acceleration model, particles are extracted from the polar cap and accelerated by large rotation-induced electric fields, forming the primary beam. The maximum potential drop that may be induced across the magnetic field lines between the magnetic pole and the last field lines that opens to infinity is $\Delta\phi = B_S R^3 \Omega^2 / 2c^2$ (Goldreich & Julian 1969), where B_S is the strength of magnetic field at neutron star surface, R is the radius of the neutron star, Ω is the angular velocity and c is the speed of light. Accordingly, for young millisecond pulsar with high magnetic fields ($B_S \sim 10^{12}$ G), the magnitude of the potential drop could be as large as $7 \times 10^{18} B_{12} P_{ms}^{-2}$ volts ($B_S \equiv B_{12} \times 10^{12}$ G). But, in young pulsars the electric field along magnetic field lines is likely to be screened well below the vacuum potentials by the onset of electron–positron pair cascades in the strong magnetic field (Cheng & Ruderman 1977), and this would limit the potential to about 10^{12} eV. Though the flux of synchrotron radiation observed from the Crab and other PWN indicates such a possibility, questions like where in the magnetosphere are pairs created and how many are created are still not settled, and one cannot rule out the possibility that ions can reach energies equal to a significant part of the total potential drop through polar cap acceleration, particularly in view of the observation of gamma radiation of energies above tens and even hundreds of TeV from Crab and other PWN.

LB (Link & Burgio 2005, 2006) conjectured that protons or heavier ions are accelerated near the surface of a pulsar by the polar caps to PeV energies (correspond to no/little screening) when $\mu \cdot \boldsymbol{\Omega} < 0$ (such a condition is expected to hold for half of the total pulsars). When pulsar-accelerated ions interact with the thermal radiation field of pulsar, the Δ-resonance state may occur provided their energies exceed the threshold energy for the process. The threshold condition for the production of Δ-resonance state in $p\gamma$ interaction is given by

$$\epsilon_p \epsilon_\gamma (1 - \cos\theta_{p\gamma}) \geq 0.3 \text{ GeV}^2, \quad (1)$$

where ϵ_p and ϵ_γ are the proton and photon energies, respectively, and $\theta_{p\gamma}$ is the incident angle between the proton and photon in the laboratory frame. In a young neutron star with surface temperature T_∞, the energy of a thermal photon near the surface of the neutron star is $2.8\,kT_\infty(1 + z_g)$, $z_g(\sim 0.4)$ being the gravitational redshift. This implies that in a young pulsar atmosphere, the condition for the production of the Δ-resonance is $B_{12} P_{ms}^{-2} T_{0.1\,keV} \geq 3 \times 10^{-4}$ (Link & Burgio 2005, 2006) where $T_{0.1\,keV} \equiv (kT_\infty / 0.1 \text{ keV})$, $T_\infty \sim 0.1$ keV being the typical surface temperature of young pulsars. Such a condition holds for many young pulsars, and thus Δ-resonance should be reached in pulsar atmosphere. Gamma-rays and neutrinos are subsequently produced through the following channels

$$p + \gamma \rightarrow \Delta^+ \rightarrow \begin{cases} p + \pi^o \rightarrow p + 2\gamma \\ n\pi^+ \rightarrow n + e^+ + \nu_e + \nu_\mu + \bar{\nu_\mu} \end{cases}.$$

Since the charge-changing reaction takes place just one-third of the time, on the average four high-energy gamma-rays are produced for every three high-energy neutrinos (or for a muon neutrino antineutrino pair) when a large number of such reactions occur.

The flux of gamma-rays and muon neutrinos from pulsars can be estimated as follows. The charge density of ions near the pulsar surface is $\rho_q \simeq eZn_o$, where $n_o(r) \equiv B_S R^3 \Omega / (4\pi Zecr^3)$ is the Goldreich–Julian density (Goldreich & Julian 1969) of ions at radial distance r. For acceleration to take place, there must be a charge-depleted gap (here polar gap), and the density in the gap may be written as $f_d(1 - f_d)\, n_o$, where $f_d (< 1)$ is the depletion factor which is a model-dependent quantity ($f_d = 0$ corresponds to zero depletion). The flux of protons accelerated by a polar cap is therefore

$$I_{pc} = c f_d (1 - f_d) n_o A_{pc}, \quad (2)$$

where $A_{pc} = \eta\, 4\, \pi\, R^2$ is the area of the polar cap, η is the ratio of the polar cap area to the neutron star surface area, which is taken as unity by LB in their work (i.e. in the original calculation by LB A_{pc} was taken to be equal to the surface area of the whole neutron star). The canonical polar cap radius is given by $r_{pc} = R(\Omega R/c)^{1/2}$ (Beskin et al. 1993), and thus

$$\eta = \Omega R / (4c). \quad (3)$$

The protons accelerated by a polar cap will interact with the thermal radiation field of the neutron star. The temperature of polar caps is expectedly higher than the surface temperature of neutron star, but the contribution of polar caps on the thermal radiation field of a neutron star should be negligible because of their small surface area in comparison with the surface area of the whole neutron star. For a young neutron star with surface temperature T_∞, the photon density close to the neutron star surface is $n_\gamma(R) = (a/2.8k)[(1 + z_g)T_\infty]^3$, a being the Stefan–Boltzmann constant. Numerically, $n_\gamma(R) \simeq 9 \times 10^{19} T_{0.1\,keV}^3$. At radial distance r, the photon density will be $n_\gamma(r) = n_\gamma(R)(R/r)^2$. The probability that a PeV energy proton starting from the pulsar surface will produce Δ particle by interacting with thermal field is given by (Link & Burgio 2005) $P_c = 1 - \int_R^r P(r)$, where $dP/P = -n_\gamma(r)\, \sigma_{p\gamma}\, dr$. The threshold energy for the production of Δ-resonance state in $p\gamma$ interaction as given by equation (1) increases rapidly with distance from the surface of neutron star because of the $(1 - \cos\theta_{p\gamma})^{-1}$ factor (Link & Burgio 2005). Requiring conversion to take place in the range $R \leq r \leq 1.2R$ [at $r = 1.2R$, the value of $(1 - cos\theta_{p\gamma})^{-1}$ averaged over surface becomes double], P_c has been found as $\simeq 0.02\, T_{0.1\,keV}^3$ (Link & Burgio 2005). From a followup calculation by Link & Burgio (2006), it is found that conversion probability is slightly lower than that mentioned above and can be parametrized as $P_c \simeq T_{0.1\,keV}^3$. Thus, the total flux of neutrino/gamma-ray generated in pulsar from the decay of Δ^+ resonance is

$$I = 2c\xi A_{pc} f_d (1 - f_d) n_o P_c, \quad (4)$$

where ξ is 4/3 and 2/3 for gamma-rays and muon neutrinos, respectively. Denoting the duty cycle of the gamma-ray/neutrino beam as

f_b (typically $f_b \sim 0.1-0.3$), the phase-averaged gamma-ray/neutrino flux at the Earth from a pulsar of distance d is given by

$$\phi \simeq 2c\xi\zeta\eta f_b f_d(1-f_d)n_o\left(\frac{R}{d}\right)^2 P_c, \quad (5)$$

where ζ represents the effect due to neutrino oscillation (the decays of pions and their muon daughters result in initial flavour ratios $\phi_{\nu_e}:\phi_{\nu_\mu}:\phi_{\nu_\tau}$ of nearly 1:2:0 but at large distance from the source the flavour ratio is expected to become 1:1:1 due to maximal mixing of ν_μ and ν_τ.). $\zeta = 1$ and 1/2 for gamma-rays and muon neutrinos, respectively.

Average energy of the produced muon neutrinos would be $\epsilon_{\nu_\mu} \sim 50\,T_{0.1\,\mathrm{keV}}^{-1}$ TeV (Link & Burgio 2005, 2006) whereas for gamma-rays it is expected to be $E_\gamma \sim 100\,T_{0.1\,\mathrm{keV}}^{-1}$ TeV.

3 TEV GAMMA-RAYS FROM A FEW POTENTIAL PULSARS: COMPARISON WITH OBSERVATIONS

Though there are about 1800 pulsars known through radio detections, only a few have been detected in the gamma-rays. From observations made with gamma-ray telescopes on satellites so far, only seven high-confidence gamma-ray pulsars are known in the energy range up to a few GeV (Thompson 2003). Besides, three other pulsars (PSR B1046−58, B0656+14 and J0218+4232) are considered to be gamma-ray emitters with a lower confidence level (Thompson 2003) in the same energy region. Some basic properties of the high-confidence *young* gamma-ray pulsars, namely distance (D), spin-down age, period (P), the calculated magnetic field strength at the neutron star surface, surface temperature and pulsar duty cycle (f_b), are listed in Table 1.

None of the listed pulsars is, however, detected at TeV energies despite recent improvement in the knowledge of Galactic gamma-ray sky above 100 GeV, mostly by means of ground-based Imaging Atmospheric Cherenkov telescope systems such as the Collaboration of Australia and Nippon for a Gamma Ray Observatory in the Outback (CANGAROO), High Energy Gamma Ray Astronomy (HEGRA), High-Energy Stereoscopic System (HESS) or the Major Atmospheric Gamma-ray Imaging Cherenkov Observatory (MAGIC). Up to now, no evidence for pulsed emission from any other pulsar has been found from the observations (Chadwick et al. 2000; Lessard et al. 2000; de Naurois et al. 2002; Aharonian et al. 2004, 2007), and only upper limits on the pulsed very high energy gamma-ray flux are derived under various assumptions on the characteristics of the pulsed emission. For the pulsars listed in Table 1, the observed upper limits of integral fluxes are given in Table 2. The upper limits are obtained from the differential spectra assuming a power-law differential spectrum with index −2.4. The upper limits of integral fluxes of gamma-rays from the pulsars at around 100 TeV as obtained by the extensive air shower experiments such as the Tibet (Amenomori et al. 2008; Wang et al. 2008) are found less restrictive.

Table 1. The characteristics of high-confidence young low-energy gamma-ray pulsars.

Source	d (kpc)	age (yr)	p (ms)	B_{12}	$T_{0.1\,\mathrm{keV}}$	f_b
Crab	2	10^3	33	3.8	∼1.7	0.14
Vela	0.29	$10^{4.2}$	89	3.4	0.6	0.04
$B\,1706-44$	1.8	$10^{4.3}$	102	3.1	1	0.13
$B\,1509-58$	4.4	$10^{3.2}$	151	0.26	1	0.26
$J\,0205+64$	3.2	$10^{2.9}$	65	3.8	0.04	0.9

Assuming that pulsar-accelerated ions are protons, numerical values of the integral TeV gamma-ray fluxes are obtained for the pulsars listed in Table 2 from equation (5) and are also shown in the same table (for the numerical estimation of flux, we take $Z = 1$ and $f_d = 1/2$ throughout this work).

It is clear from Table 2 that the model with $\eta = 1$ is not consistent with the observed upper limits; the observed limits are substantially lower than the predicted fluxes. The observations made so far, however, do not rule out the model with η given by equation (3).

4 TEV NEUTRINOS FROM PULSARS

When η is given by equation (3), neutrino fluxes from nearby young gamma-ray pulsars would be much lower than estimated by LB (Link & Burgio 2006). A high-energy muon neutrino is usually detected indirectly through the observation of the secondary high-energy muon produced by the muon neutrino on interaction with the ice or rock in the vicinity of a neutrino telescope via charged current interactions. The track of the produced muon is usually reconstructed by detecting the Cerenkov light emitted by the muon as it propagates through the telescope. The probability of the detection of muon neutrinos is the product of the interaction probability of neutrinos and the range of the muon and is $p_{\nu\to\mu} \simeq 1.3\times10^{-6}(\epsilon_{\nu_\mu}/1\ \mathrm{TeV})$ (Gaisser, Halzen & Stanev 1995). The expected event rates in a neutrino telescope due to potential young pulsars are given in Table 3.

The event rates are clearly very low and thus possibility of observing pulsars by a kilometre-scale neutrino detector does not look bright.

5 GAMMA-RAYS AND NEUTRINOS FROM PULSAR NEBULA

A young neutron star is generally encircled by PWN. Positive ions, after gaining energy from polar gaps, will move away from the pulsar practically along the open field lines and will finally inject into the nebula. It is very likely that these energetic ions would be trapped by the magnetic field of the nebula for a long period and consequently they should produce appreciable high-energy gamma-rays/neutrinos by interacting with the matter of the nebula.

5.1 Magnetic trapping of pulsar-accelerated PeV ions in nebulae

Conservation of magnetic flux across the light cylinder entails that outside the light cylinder $B \sim r^{-1}$ whereas far from the light cylinder the radial component of magnetic field varies as $B_r \sim r^{-2}$. Thus, (far) outside the light cylinder the azimuthal component of the magnetic field dominates over the radial field. Therefore, accelerated protons while moving away from the pulsar have to cross the field lines (e.g. magnetic field lines at wind shock). The Larmor radius of particles (even for proton) of energy about 1 PeV is expected to be smaller than the radius of nebula during most of the time of the evolution of nebula (Bednarek & Protheroe 2002; Bhadra 2006). Thus, it is very likely that energetic particles of PeV energies would be trapped by the magnetic field of the nebula. The energetic particles propagate diffusively in the envelope, and they escape from nebula when the mean radial distance travelled by the particles becomes comparable with the radius of nebula at the time of escaping. This time is somewhat uncertain due to the uncertainty of the value of

Table 2. Comparison of predicted versus observed integral TeV gamma-ray fluxes from some nearby young gamma-ray pulsars. The numbers in parentheses are the energy thresholds in TeV for which upper limits are determined. The observed upper limits for Crab pulsar are due to Aharonian et al. (2006a) whereas for the rest of the pulsars the observed upper limits are due to Aharonian et al. (2007).

Source	Expected integral flux		Observed upper limit of integral flux
	$\eta = 1$ (10^{-15} cm^{-2} s^{-1})	η as given by equation (3) (10^{-15} cm^{-2} s^{-1})	(10^{-15} cm^{-2} s^{-1})
Crab	1012	1.65	8 (56)
Vela	208	0.123	10 (20)
B 1509 − 58	67	0.0034	10 (20)
B 1706 − 44	71	0.0025	10 (20)

Table 3. Expected event rates in a neutrino telescope due to some nearby young gamma-ray pulsars.

Source	Expected event rates (km^{-2} yr^{-1})
Crab	0.009
Vela	0.0007
B 1509 − 58	0.00003
B 1706 − 44	0.00003

diffusion coefficient, but is estimated to be at least a few thousand years (Bednarek & Protheroe 2002; Bhadra 2006).

5.2 Gamma-rays and neutrinos from nebulae of young pulsars

As pointed out in the preceding section, the pulsar-injected ions of PeV energies should be trapped by the magnetic field of the nebula for a long period, and consequently there would be an accumulation of energetic ions in the nebula. These energetic ions will interact with the matter of the nebula. The rate of interactions (ξ) would be $nc\,\sigma_{pA}$, where n is the number density of protons in nebula and σ_{pA} is the interaction cross-section. In each such interaction, charged and neutral pions will be produced copiously. Subsequently, the decays of neutral pions will produce gamma-rays whereas charged pions and their muon daughters will give rise to neutrinos.

If m is the mean multiplicity of charged particles in proton–ion interaction, then the flux of gamma-rays at a distance d from the source would roughly be

$$\phi_\gamma \approx 2c\beta\eta f_d(1 - f_d)n_o \left(\frac{R}{d}\right)^2 \xi m t, \qquad (6)$$

where β represents the fraction of pulsar-accelerated protons trapped in the nebula and t is the age of the pulsar. Note that there should not be any reduction of flux due to pulsar duty cycle in the case of emission to nebula. Though n_o is taken as constant, but actually at the early stages of pulsar n_o should be larger owing to the smaller pulsar period. So, the above expression gives only a lower limit of flux. Typical energy of these resultant gamma-rays would be $\sim 10^3/(6m)$ TeV where for (laboratory) collision energy of 1 PeV m is about 32 (Alner et al. 1987).

Numerical values of the integral TeV gamma-ray fluxes from two nearby nebulae, Crab nebula and Vela nebula, have been estimated for perfect trapping of pulsar-accelerated protons in nebulae and are shown in Table 4. The observed integral gamma-ray fluxes above 1 TeV from Crab nebula (Aharonian et al. 2006a) and Vela nebual (Aharonian et al. 2006b) are also given in Table 4 for comparison.

Table 4. Comparison of predicted versus observed integral gamma-ray fluxes from two nearby PWN.

PWNe	n (cm^{-3})	Expected flux ($\times 10^{-12}$ cm^{-2} s^{-1})	Observed flux (10^{-12} cm^{-2} s^{-1})
Crab nebula	150	0.6	22.6
Vela nebula	1	0.4	12.8

The neutrino fluxes from the nebulae would be of nearly the same to those of gamma-rays. Incorporating the neutrino oscillation effect, the expected event rates in a neutrino telescope due to TeV muon neutrinos from nebulae of Crab and Vela are 0.2 and 0.1 km^{-2} yr^{-1}, respectively. Note that the event rates obtained here are rough numerical values. The flux will be higher if the accelerated ion is heavier than proton.

6 CONCLUSION

To summarize, this work suggests that pulsars are unlikely to be strong sources of TeV neutrinos. The non-detection of any statistically significant excess from the direction of any pulsar by the Antarctic Muon and Neutrino Detector Array (AMANDA)-II telescope (Ahrens et al. 2004; Ackermann et al. 2005, 2008) is thus as per expectations.

If protons are accelerated to PeV energies by the pulsar, then pulsar nebulae are more probable sites of energetic neutrinos provided energetic particles of PeV energies are efficiently trapped by the magnetic field of the nebulae. But, even for pulsar nebulae the expected event rates are small and the detection probability of pulsar nebulae by the upcoming neutrino telescopes, such as the IceCube (Halzen 2006), is very low.

ACKNOWLEDGMENTS

The authors would like to thank an anonymous referee for very useful comments and suggestions.

REFERENCES

Ackermann M. et al., 2005, Phys. Rev. D, 71, 077102
Ackermann M. et al., 2008, ApJ, 675, 1014
Aharonian F., et al. (HEGRA collaboration), 2004, ApJ, 614, 897
Aharonian F. et al. (HESS Collaboration), 2006a, Astron. Astrophys., 457, 899

Aharonian F. et al. (HESS Collaboration), 2006b, Astron. Astrophys., 448, 206
Aharonian F. et al. (HESS collaboration), 2007, Astron. Astrophys., 466, 543
Ahrens J. et al., 2004, Phys. Rev. Lett., 92, 071102
Alner G. J. et al., 1987, Phys. Rep., 154, 247
Amenomori M. et al. (Tibet ASgamma Collaboration), 2008, Nucl. Phys. Proc. Suppl., 175-176, 431
Arons J., Scharlemann E. T., 1979, ApJ, 231, 854
Bednarek W., Protheroe R. J., 2002, Astropart. Phys., 16, 397
Beskin V. S., Gurevich A. V., Istomin N. Ya., 1993, Physics of the Pulsar Magnetosphere. Cambridge Univ. Press, Cambridge, p. 117
Bhadra A., 2006, Astropart. Phys., 25, 226
Chadwick P. M., Lyons K., McComb T. J. L., Orford K. J., Osborne J. L., Rayner S. M., Shaw S. E., Turver K. E., 2000, ApJ, 537, 414
Cheng K. S., Ruderman M., 1977, ApJ, 214, 598
Cheng K. S., Ho C., Ruderman M., 1986, ApJ, 300, 500
Daugherty J. K., Harding A. K., 1996, ApJ, 458, 278
de Naurois M. et al., 2002, ApJ, 566, 343
Gaisser T. K., Halzen F., Stanev T., 1995, Phys. Rept., 258, 173
Goldreich P., Julian W. H., 1969, ApJ, 157, 869
Halzen F., 2006, Eur. Phys. J. C, 46, 669
Halzen F., Hooper D., 2002, Prog. Theor. Phys., 65, 1025
Harding A. K., Muslimov A. G., 1998, ApJ, 508, 328
Lessard R. W. et al., 2000, ApJ, 531, 942
Link B., Burgio F., 2005, Phys. Rev. Lett., 94, 181101
Link B., Burgio F., 2006, MNRAS, 371, 375
Ruderman M. A., Sutherland P. G., 1975, ApJ, 196, 51
Thompson D. J., 2003, preprint (astro-ph/0312272)
Wang Y. et al., 2008, preprint (astro-ph/ 08041862)

This paper has been typeset from a TEX/LATEX file prepared by the author.

Imprint of Geomagnetic field on charged particle distribution in EAS

J.N. CAPDEVIELLE[1,2], R.K. DEY[2], A. BHADRA[3]
[1]*APC, Univ. Paris-Diderot, Bt. Condorcet, 10 rue Alice Domon 75205 Paris Cedex 13 France*
[2]*Dept of Physics, Univ. of North Bengal, Siliguri, WB 734013 India*
[3]*High Energy and Cosmic Ray Research Centre, Univ. of North Bengal, Siliguri, WB 734013 India*
capdev@apc.univ-paris7.fr
DOI: 10.7529/ICRC2011/V01/1127

Abstract: The standard perception is that the muons and othercharged particles in cosmic ray extensive air shower (EAS) are distributed symmetrically about the shower axis. However, from an analysis of Monte Carlo simulation data it is revealed that an asymmetry may develop in both positive and negative muon numbers about the shower axis depending on the geomagnetic field at the location of the observation. Such an asymmetry is particularly pronounced at certain zenith and azimuth angle range. The electron component of EAS also carries such an impression but with a smaller magnitude. Such an effect of geomagnetic field is found to enhance with the mass of the shower initiating particles.

Keywords: geomagnetic field, EAS electron and muon distributions, barycenters of positive and negative particles

1 Muon component and geomagnetic field

An advantageous feature of CORSIKA [1] is that particles and anti-particles can be followed separately and individually. Hence in a Monte Carlo simulation study using CORSIKA one can follow positive and negative muons during propagation in the atmosphere, as well as on arrival at ground level: muons are collected after charged pion double body decay and also after two-body and three-body kaon decays with the different branching ratios. The deflection of muons during their propagation in the atmosphere is caused predominantly by the multiple Coulomb scattering and the curvature of the trajectories, as for all the charged particles of the simulation, in the Earth's magnetic field.

Our first attempt concerning positive and negative muons separately was carried out at high energy for the AUGER Observatory (PAO) and also at relatively lower energies [2, 3]. In the coordinate system of CORSIKA, the magnetic field at PAO is characterized by the two geomagnetic components $B_x = 20.5\mu T$ and $B_z = -14.5\mu T$. In order to point out some typical signature of the nature of primary particle, not on the traditional muon-electron abundance, but on the contrast behavior of positive and negative particles in EAS, we calculated the barycenters of positive and negative muons, $\delta_{\mu+\mu-}$ and the orientation, $\phi_{\mu+\mu-}$ for each shower event at certain azimuthal angles.

For the soft component the radiation lengths are too short and too many scattering deviations occur and as a result the lateral spread is mainly due to the multiple coulomb scattering. Consequently the possibility of sorting out the signature of the geomagnetic field on the soft component is not much. Nethertheless, we shall explore herealso, taking all the advantages of the EGS option, the possible differences between proton and heavy nuclei induced showers revealing in the electron and positron component.

In the case of EAS muons, especially for heavy nuclei initiated showers where the muons start at higher altitude at comparatively lower energies than for proton primaries, a barycenter separation of about 200 m was obtained at UHE for vertical showers (iron primaries) using a thinning factor 10^{-6}. It appears that this separation, which is clearer in the case of nuclei, is also connected with the statistical reduction of the fluctuations of showers initiated by nuclei.

To eliminate any possible bias generated by the thinning technique and to understand more rapidly the benefit of this geomagnetic effect, a sample of few hundred showers without thinning for muons with detection threshold energies exceeding 300 MeV, was simulated and some systematic features have emerged out from the simulated data. For instance, for primary iron induced near vertical showers at 10^6 GeV, the orientation of the dipole towards East-West direction and a net barycenter separation of about 100 m have been noticed irrespective of the azimuthal angle of incidence.

A tremendously large separation of about 500 m (figure1) has been found in the case of very inclined showers ($\Theta = 55°$) at a depth of $860g/cm^2$.

The difference between heavy and light nuclei at UHE can be studied in both directions:

- ratio of μ^+,μ^- at convenient distances
- ellipticity of the muon component

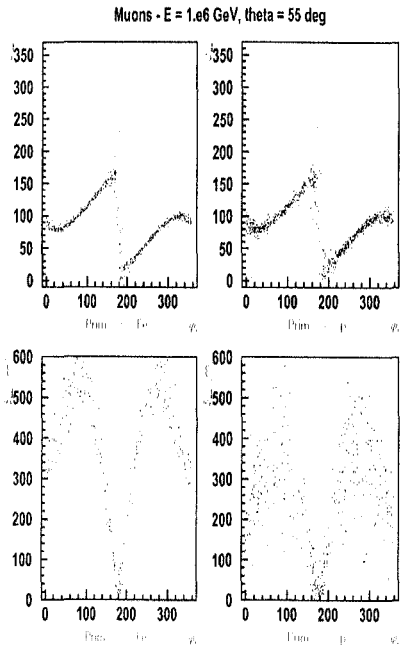

Figure 1: dependences of positive-negative muon dipole orientation $\phi_{\mu+\mu-}$ (upper part), barycenter separation $\delta_{\mu+\mu-}$ (lower part) versus azimuthal incidence ϕ_i with showers zenithal incidence at 55° .
- left side : iron initiated showers
- right side : proton initiated showers

Alternatively, in the absence of detectors for muon charge identification, we introduced the ellipticity factor $\epsilon(r) = \rho_{\mu//}(r)/\rho_{\mu\perp}(r)$, the ratio of total muon densities at the same distance from the shower axis, one on the axis oriented along the muonic dipole and the other on the axis perpendicular to it.

2 Asymmetries in electron and muon distributions

Following the stated preliminary approach, in the present calculations we have considered a sample of simulated EAS events with fixed primary energy 10^6 GeV and try to extract the nature of primaries from the distribution of charged particles (muons and electrons) in different quadrants centered about the shower core and taking the X and Y axes as North and West direction respectively following the convention used in CORSIKA.

We consider both vertical as well as large inclined showers (zenith angle $\Theta = 50°$) to clearly identify the effect of gromagnetic field which should be pronounced along the longer path. In the later case we compare showers initiated with azimutal angles $\phi = 0°$ (figure 2-left) and $\phi = 90°$

	-45 to 45°	45 to 135°	135 to 225°	225 to 315°
$e+$	346	245	503	235
$e-$	514	338	775	374
$\mu+$	916	724	1043	422
$\mu-$	877	404	1010	708

Table 1: Kascade level: number of electrons and muons in quadrants for p primary $\Theta = 50°$, $\phi = 0°$

	-45 to 45°	45 to 135°	135 to 225°	225 to 315°
$e+$	246	184	270	147
$e-$	353	233	393	231
$\mu+$	1225	1117	1387	523
$\mu-$	1211	502	1363	1095

Table 2: Kascade level: number of electrons and muons in quadrants for Fe primary $\Theta = 50°$, $\phi = 0°$

(figure 2-right). The relative muon to electron ratio $\rho(\Phi 1)$ is calculated from the muon /electron size in each quadrant normalized to the total muon/electron content for all the quadrants ($\Phi 1$ is the angle of the central axis of a given quadrant with the X axis) and the differences appearing in the tabulations for p, Fe in each sector have been revealed. This behaviour emerges from the simulation results such as presented in the table 1 at Kascade [4] location for p initiated showers and also for iron induced EAS as given in the table 2. The calculations have been performed at Kascade and Ice Top levels [5] with components of magnetic field, respectively $B_x = 20.52\mu T$, $B_z = 43.57\mu T$ and $B_x = 16.62\mu T$, $B_z = -52.55\mu T$. Note that Ice Top is situated within few meters of the geographic south pole but very far away from the geomagnetic South pole.

The same study has been made by dividing the components of the geomagnetic field by a factor of one thousand to identify the role of the other factors especially the annihilation of the positron and the capture of negative muons of low energy on asymmetries in charged partcle distribution in inclined showers. The results are shown here for muons with energies larger than 230 MeV, whereas the energy threshold for electrons is 5 MeV. We underline that Tables 1 and 2 are just a small sample illustrating general assymmetries in the different quadrant after adding in each sector all muons(positive and negative) as well as all electrons and positrons. Those large anisotropies in inclined EAS can be measured without expensive detectors needing charge separation but with normal detectors sufficient to collect important information in terms of relation between muons and geomagnetic field as well as hints of primary composition.

3 Topological analysis by the BF treatment

A basic assumption of all known hitherto codes used to analyse the data obtained with the CORSIKA and other

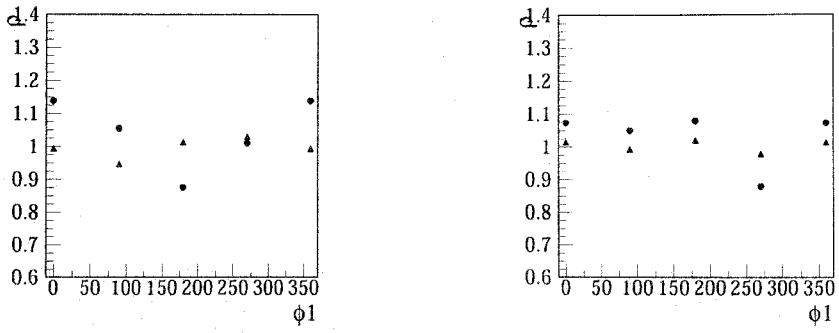

Figure 2: Relative muon electron ratio ρ in different quadrants left: EAS $\phi = 0°$ discs (proton primaries), triangles (iron primaries); right: EAS $\phi = 90°$ discs (proton primaries), triangles (iron primaries)

EAS Monte Carlo simulations is the cylindrical symmetry of charged particles in EAS and such a symmetry is normally noticed on average. In contrast the present analysis revealed an anisotropy in charged particle distribution due to geomagnetic field, particularly at higher zenith angle as stated above. To conserve the asymmetric characteristics of the charged particle distribution due to geomagnetic field, we introduce a procedure of scanning of charged particle density with the butterfly (BF) treatment in order to point out typical signatures relevant to the nature of primaries: the BF consists of two opposite wings around the shower core limited by a pair of symmetric arcs at distances which may be enlarged above $200m$ for very large EAS.

The internal angle of the wing is taken as 90°(quadrant) which can be reduced to emphasize some particular effects. The density of muons inside a wing is compared with that in different wings and the centre of gravity of charged particles (positive and negative separately) are computed from the simulation data. A large separation corresponds to a flatter distribution of the lateral distribution. It is possible to rotate the BF around the axis to identify the areas containing larger differences. The rotation of the BF is measured by the same angle $\Phi 1$ (between the central axis of the BFs and the X axis) to the case of the quadrants. One may notice the contrast between p and iron primaries characterized by a steep decrease of $\Phi 1 = 0.°$ to $\Phi 1 = 180.°$ followed by a fast increase (p primary) against a more modest variation for iron primary as shown in figure 2 . The lateral muon distributions are also calculated separately for positive and negative muons inside the different sectors and compared at both levels of Kascade and Ice Top(figure3), respectively for $\phi = 0.°$ and $\phi = 90.°$

Adopting the BF technique we have also explored the variation of the separating distances of the barycenters of positive and negative muons at both levels of Kascade and Ice Top (figure4), respectively for $\phi = 0.°$ and $\phi = 90.°$

4 Discussion

Our analysis concerning the effects of the geomagnetic field on positive and negative muon and electron components of inclined EAS reveals differences in various features such as asymmetries in sectorial distributions, sectorial muon-electron relative abundances, amplitude of fluctuations between proton and iron induced showers. Such effects are found to persist and are of comparable magnitude if we replace the Gheisha code in the simulation by the Fluka code in the treatment of low energy hadron collisions.

New estimators can be derived from the asymmetries in the profile of muons lateral distributions in different wings of the BF, especially when contrast view in different wings is considered and when the X axis of the BF is superimposed on the axis of the muon dipole : the behavior of the muon electron ratio in different sectors also carries signature discriminating light and heavy primaries. The present calculations will be extended in near future for different primary energies in order to present the results at both fixed electron or muon size.

Furthermore, our method can be implemented experimentally to identify the nature of primary particle with the employment of large muon detectors able to distinguish positive and negative particles at distances of $10 - 50m$ in an EAS array.

References

[1] J. N. Capdevielle et al. KfK report-4998, ed. KfK*The Extensive Air Shower Simulation Code CORSIKA*, Karlsruhe (1992) and report-6019(1998) ed. FZK
[2] J.N. Capdevielle et al., Astrop.Phys., 13, 259(2000)
[3] J.N. Capdevielle, 1st Arctic Workskop on C. R. Muons, Sodankyla, Finland (1999)
[4] W D Apel et al., Astropart. Phys. 24, 467 (2006)
[5] T. Stanev, Nucl.. Phys. B,196,159, 164 (2009)

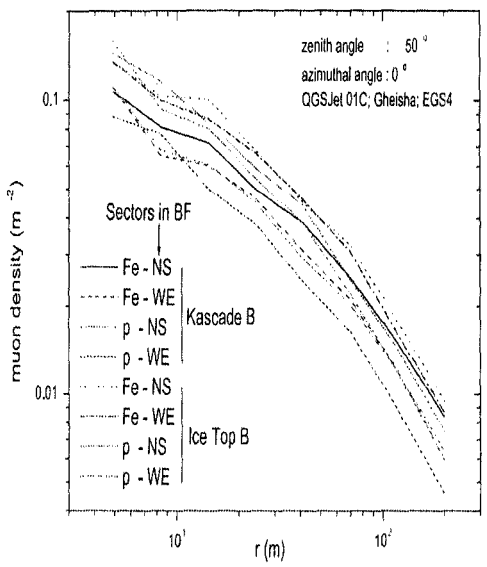

Fig.3

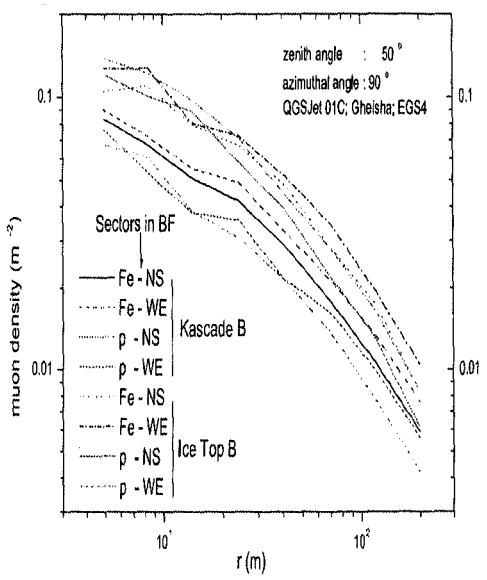

Fig.5

Figure 3: Lateral muon distributions in different sectors.Left: for $\theta = 50°$ and $\phi = 0°$. Upper curves for Ice Top array, lower curves for Kascade level. Right : the same for $\phi = 90°$.

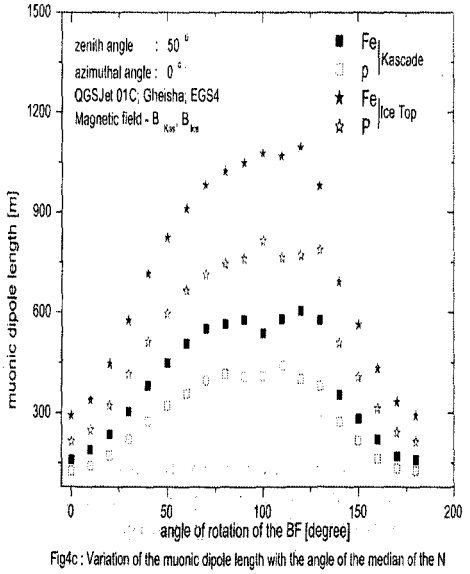

Fig4c : Variation of the muonic dipole length with the angle of the median of the N sector of the BF with OX axis of the CORSIKA coordinate at Kascade & Ice Top sites.

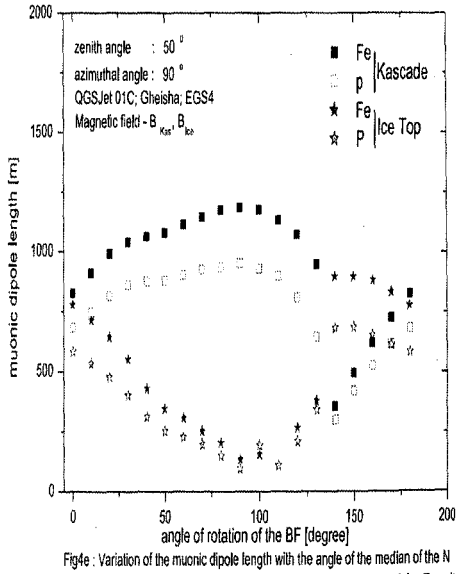

Fig4e : Variation of the muonic dipole length with the angle of the median of the N sector of the BF with OX axis of the CORSIKA coordinate at Kascade & Ice Top sites.

Figure 4: Distance between positive Mu+ and negative Mu- barycenters in different sectors. Left: for $\theta = 50°$ and $\phi = 0°$. Upper curves for Ice Top array, lower curves for Kas cade level. Right : the same for $\phi = 90°$.

Primary mass sensitivity of lateral shower age parameter in EAS

R.K. DEY[1], A. BHADRA[2], J.N. CAPDEVIELLE[3]
[1]*Dept of Physics, Univ. of North Bengal, Siliguri, WB 734013 India*
[2]*High Energy and Cosmic Ray Research Centre, Univ. of North Bengal, Siliguri, WB 734013 India*
[3]*APC, Univ. Paris-Diderot, Bt. Condorcet, 10 rue Alice Domon 75205 Paris Cedex 13 France*
rkdey2007phy@rediffmail.com
DOI: 10.7529/ICRC2011/V01/0107

Abstract: Detailed Monte Carlo simulation studies of cosmic ray extensive air showers in the energy range 0.1 PeV - 1 EeV are made using CORSIKA in order to examine the sensitivity of lateral shower age to primary mass. After proposing an unambiguous way of estimating lateral shower age parameter, a few measurable properties of the lateral shower age and its correlation with other EAS observables are studied for different primaries using the Monte Carlo simulated data, which demonstrate clear mass dependence. The findings from simulation are compared with some experimental results to extract information on average mass composition around the knee region.

Keywords: cosmic ray, EAS, lateral shower age

1 Introduction

The lateral density distribution of electrons in cosmic ray extensive air shower (EAS) is usually approximated by the well known Nishimura-Kamata-Greisen (NKG) structure function [1] and the shower parameters viz. shower size which is the total number of electrons in an EAS and shower age ($s_\perp$) that describes the slope of the radial distribution of electrons in EAS are evaluated by fitting the structure function with the measured densities. While shower size is often related with the energy of the EAS initiating particle but the lateral shower age has not received sufficient importance so far in deducing information on primaries from EAS observations. This is probably because the lateral shower age estimated from experimental data differs from the longitudinal age (s_L) that describes the developmental stage of a cosmic ray cascade in atmosphere. Note that theoretically $s_\perp$ is supposed to be equal to s_L. It is further observed that the NKG function with a single lateral age parameter is insufficient to describe the experimental lateral distribution of EAS electrons properly at all distances implying that the lateral age changes with radial distance.

Some experimental results [2, 3], however, suggests that two age parameters are connected through the approximate relation $s_L \geq s_\perp + \delta$, with $\delta \approx 0.2$. Some early Monte Carlo (MC) simulation studies [4] also indicate that the lateral age has some correlation with longitudinal age and hence the parameter should be sensitive on the nature of the shower initiating particle. In recent years the knowledge of high energy interactions has been improved a lot with the accelerator results. Consequently uncertainties on the results of MC studies of EAS have been reduced significantly at present.

In the present work we would explore through MC study whether lateral age parameter is sensitive on primary mass and consequently the possible role that the parameter may play in a multi-parameter approach of studying EAS to understand the nature of shower initiating particles. One major challenge, however, is the reliable and unambiguous estimation of the lateral shower age from the experimentally measured electron densities. We would address this problem first.

2 Lateral age parameter

The lateral density distribution of cascade particles can be approximated by the well known Nishimura-Kamata-Greisen (NKG) structure function proposed by Greisen [1], which is given by

$$f(r) = C(s_\perp)(r/r_m)^{s_\perp - 2}(1 + r/r_m)^{s_\perp - 4.5}\,, \qquad (1)$$

where r is the radial distance from the shower core, r_m is the Molière radius which is nearly $80m$ at sea level, and the normalization factor $C(s_\perp)$ is given by

$$C(s_\perp) = \frac{\Gamma(4.5 - s_\perp)}{2\pi\Gamma(s_\perp)\Gamma(4.5 - 2s_\perp)}\,. \qquad (2)$$

The NKG formula has the advantage of normalization as it is integrable in Euler Beta function. The normalization of

f(r) implies for the electron density $\rho(r) = N_e f(r)$. But such a handy relation does not hold if $s_\perp$ varies with r, as noted in several observations.

An improvement of the NKG function was proposed by adopting a modulated, longitudinal age parameter s_L dependent effective Moliere radius so that

$$\rho_{el}(r) = (mr_m)^{-2}\rho_{NKG}(r/m) \qquad (3)$$

where $m = 0.78 - 0.21s_L$. But even with such a modification lateral age is found to vary with radial age experimentally. To handle the situation a method was developed by Capdevielle et al. [4] introducing the notion of local age parameter.

From two neighbouring points, i and j, we can give a (local) lateral age parameter for any distribution $f(x)$ (where $x = \frac{r}{r_m}$) which characterizes the best fit by a NKG-type function in $[x_i, x_j]$:

$$s_{ij} = \frac{\ln(F_{ij}X_{ij}^2Y_{ij}^{4.5})}{\ln(X_{ij}Y_{ij})} \qquad (4)$$

where $F_{ij} = f(r_i)/f(r_j)$, $X_{ij}=r_i/r_j$, and $Y_{ij}=(x_i+1)/(x_j+1)$. More generally, if $r_i \to r_j$, this suggests the definition of the LAP $s(x)$ (or $s(r)$) at each point :

$$s(r) = \frac{1}{2x+1}\left((x+1)\frac{\partial \ln f}{\partial \ln x} + 6.5x + 2\right) \qquad (5)$$

Function $f_{NKG}(r)$ with s=$s(r)$ can be used to fit f in the neighbourhood of r.

The identification $s(r) = s_{ij}$ for $r = \frac{r_i+r_j}{2}$ remains valid for the experimental distributions (taking $F_{ij} = \rho(r_i)/\rho(r_j)$ as far as they are approximated by monotonic decreasing functions versus distance.

The behavior of the local age parameter s_{Loc} on experimental lateral distributions was found in accordance with the prediction [4] which was reaffirmed by the Akeno observations [5]. The stated method was validated by the rapporteurs of the ICRC from 1981 to 1985 [6]. The whole procedure was also employed in the calculation of radio effects of EAS.

In the present work we would consider local (lateral) age parameter.

3 Generation of EAS events

For generating EAS events, the air shower simulation program CORSIKA (COsmic Ray SImulation for KAscade) version 6.600 and 6.735 [7] is exploited here in the energy range from 0.1 PeV to 1 EeV. The high energy (above 80GeV/n) hadronic interaction model QGSJET 01 version 1c [8] has been used in combination with the low energy (below 80GeV/n) hadronic interaction model GHEISHA (version 2002d) or FLUKA [9] depending on the primary energy. For the electro-magnetic part both the EGS4 program library and the NKG option are used. We consider the US-standard atmospheric model [10] with planar approximation. The maximum primary zenith angle is restricted to 50°. The EAS events have been generated mainly for Proton and Iron nuclei as primaries. A small number of events have also been simulated for He primaries.

4 Estimation of lateral shower age

The simulated data have been analyzed using the reconstruction algorithms developed to obtain basic shower parameters i.e. shower size (total number of shower electrons) and shower age. We adopt two different methods. First following the traditional approach we estimate basic shower parameters by fitting the density data with the NKG structure function. Secondly, exploiting Eq.(4) we directly estimate local shower age parameter for each individual event.

We noted that the description of the data by the NKG function is improved a lot when the Moliere radius is treated as a variable rather than a fixed parameter. But this better description comes at the expense of very high shower age value which somewhat obscures the physical meaning of the age parameter as assigned in the cascade theory.

The variation of local age parameter with radial distance from the shower core is shown in figure 1(Left) for proton and iron primaries. It is known from previous studies [4] that the local age parameter initially decreases with radial distance, reaches a minimum between 30 to 50 m and then increases with radial distance. Here we have noticed two other interesting features: The local age again starts to decrease around 300 m and more importantly the nature of the variation of local age with radial distance appears nearly the same for all primary energies i.e. the nature of variation is practically independent of energy of the shower initiating particles. This decrease of s(r) around 300 m has been noticed in Akeno [5] and in Kascade-Grande [11].

Such a behaviour is also confirmed experimentally in figure 1(Right) of Kascade report [12]: this figure exhibits a maximal deficit at 50-80m in the ratio of measured and fitted electron densities, as well as an excess at large distances when fitting with NKG formula. Here we have compared the radial variation of local age obtained out of the simulated data for proton and iron primaries with those obtained from the experimentally measured density distribution data of KASCADE in figure 2.

5 The correlation of shower age parameter with other EAS observables

To explore the physical nature associated with lateral shower parameter, if any, we study some characteristics of shower age. We consider local age at two different conditions, the minimum value of local age that corresponds to

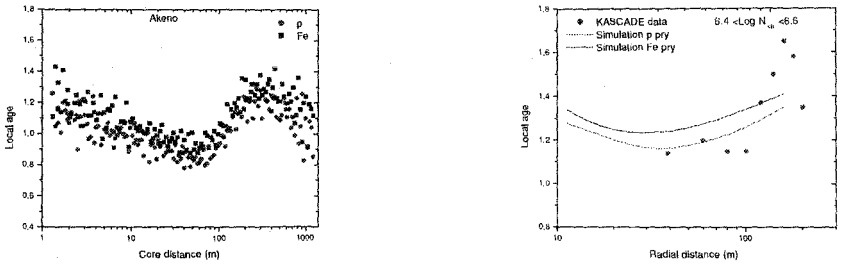

Figure 1: Left: Local age parameter obtained from simulated data as a function of radial distance for proton and Fe primaries at Akeno site at energy 10^{18} eV; Right: The radial variation of local age obtained from the KASCADE observed lateral distribution data.

local age at about radial distance 50 m and a some sort of average between 50 m to 200 m.

The variation of local shower age with shower size for the zenith angle interval (0^o - 45^o) is presented in figure 2 for KASCADE location. It is noticed that the local age decreases with shower size but the rate of decrease slows down at higher shower size. With increasing primary energy i.e. with increasing shower size showers penetrate deeper into the atmosphere resulting in steeper lateral distribution indicated by the smaller lateral shower age parameter. The simulation results show that showers induced by heavier primaries are older compared to those generated by light primaries. When the simulation results are compared with the experimental data, the KASCADE observations indicate for a change in mass composition towards heavier nuclei around the knee.

The fluctuations (variance) of local shower age in different shower size bins are estimated and the shower age fluctuations as a function of shower size are drawn in figure 3 for proton and iron primaries. It is found that at higher energies fluctuations in local shower age is larger for proton initiated showers in compare to those initiated by primary Fe which is in accordance to the predictions of early works [13] but at lower energies a reverse trend has been noticed. In figures 4 we plot the 3-dimensional curve between average local shower age at a radial distance about 40 m (minimum value), average shower size and mean muon size obtained from simulation results for both proton and iron primaries at Akeno and KASCADE location. The corresponding observational results of the Akeno and KASCADE experiments are also shown. For the Akeno experimental data we extract the minimum local age for different shower sizes from a paper [5] whereas the mean muon content corresponding to those shower sizes are obtained from reference. In the case of KASCADE data, we estimated local age from their measured lateral distribution and corresponding muon size are extracted from the $N_e - N_{mu}$ curve.

The comparison of simulated results with experimental observation from both the Akeno and KASCADE EAS experiments (figure 4) indicate for a change in primary composition towards heavier primary as energy increases across

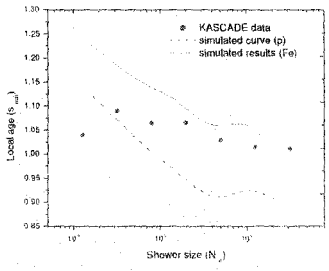

Figure 2: Variation of local age with shower size.

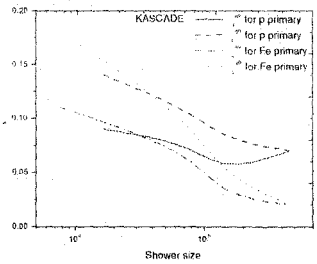

Figure 3: Fluctuation of shower age as a function of shower size.

the knee of the primary energy spectrum. The KASCADE group also reached at the similar conclusion using slope parameter instead of shower age.

6 Conclusions

The present analysis sugests that the local age parameter offers a good solution toward unambiguous estimation of shower age parameter. Since the local age parameter is found to vary with radial distance, comparison of age parameters obtained by different EAS experimental groups is

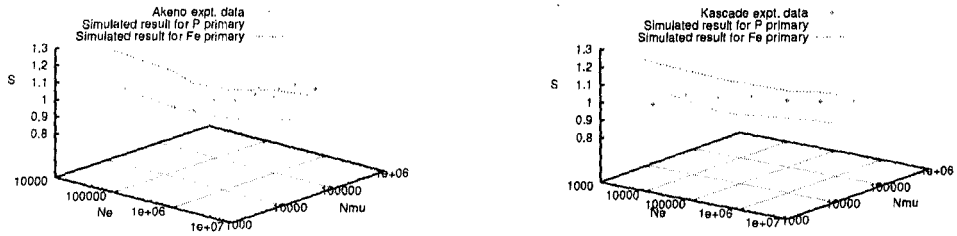

Figure 4: 3-Dimensional plot between shower size, muon size and lateral shower age for proton and Fe primaries at Akeno and KASCADE locations.

difficult as the radius of the shower disc differ from experiment to experiment. Local age at a particular distance (say at the position of minimum i.e. around core distance 40 m) is however, problematic owing to the large fluctuation of electron density data in EAS in a real measurement. We, therefore, propose to take some sort of average local age between the first minimum at around core distance of 40 m and the subsequent local maximum at around 300 m.

The local shower age takes higher value for iron initiated showers in compare to that of proton initiated showers which means that lateral distribution of electrons for iron initiated EAS is flatter relative to that of proton initiated EAS. The slope of lateral shower age versus atmospheric depth curve is, however, more or less the same for proton and iron initiated EAS.

The fluctuation of local/lateral shower age parameter has been found quite sensitive to the nature of primary particle. However, the level uncertainty in determining lateral shower age, particularly in experiments, is comparable with the magnitude of fluctuation and hence deriving any firm conclusion on the nature of primary from the study of fluctuation of lateral shower age alone is difficult.

For the study of primary composition the 3-dimensional plot of shower size versus muon size and shower age seems to offer better accuracy in compare to the more conventional approach of implementing it through the shower size versus muon size curve. It would be an interesting task to apply such 3-dimensional plot to obtain the composition of primary cosmic rays using observed EAS data from a closely packed air shower array with the facility of concurrent muon measurements such as the GRAPES experiment at Ooty [14].

Theoretically the total muon content in an EAS is a strong mass sensitive parameter. However, it is revealed from many experimental studies that it is not always possible to extract proper information on primary mass from the muon content alone. This is mainly due to the limited muon detection area in a real EAS experiment and EAS fluctuations. The present findings suggest that simultaneous study of magnitude of lateral age, its fluctuation and the 3-dimensional variation of the parameter with electron and muon content of EAS may assist to extract the nature of the shower initiating particle with a better accuracy.

References

[1] K Greisen, Progress in Cosmic Ray Physics, Vol.III, Amsterdam, NH publishing Co 1956

[2] L. G. Dedenko *et al.*, Proc. 14th Int. Cosmic Ray Conf. (Munchen) vol 8, p. 2731 (1975)

[3] J N Stamenov, Proc. 20th Int. Cosmic Ray Conf. (Moscow) vol 8, p. 258 (1987).

[4] J.N. Capdevielle and J. Gawin, J. of Physics G,8, 1317 (1982)

[5] M. Nagano et al., Journal of the physical society of Japan, vol. 53, pp.1667-1681 (1984)

[6] S. Tonwar, Proc. 17^{th} ICRC, Paris, 13, 330 (1981); M.V. Rao, Proc. 18^{th} ICRC,Bangalore 11 (1983)

[7] D. Heck et al., FZK A report-6019 ed. FZK *The CORSIKA Air Shower Simulation Program*, Karlsruhe (1998)

[8] N N Kalmykov, S S Ostapchenko et al., Nucl. Phys. B (Proc. Suppl.) 52,17 (1997)

[9] H Fesefeldt Report PITHA-85/02 (RWTH Aachen)(1985); A Ferrari and P R Sala ATLAS int. note PHYS-N0-086(CERN,Geneva)(1996)

[10] NASA, U.S.Standard Atmosphere, Tech.Rep.NASA-TM-X-74335(1976)

[11] J.N. Capdevielle et al., J.Phys. G : Nucl. Part. Phys., 31 , 507-524(2005)

[12] T Antoni, et al., Astropart. Phys. 14, 245 (2001)

[13] M Nagano et al., J. Phys. G, 10(1984), 1295-1310

[14] S K Gupta et al., Nucl. Instrum. and Methods. A 540, 311 (2005)

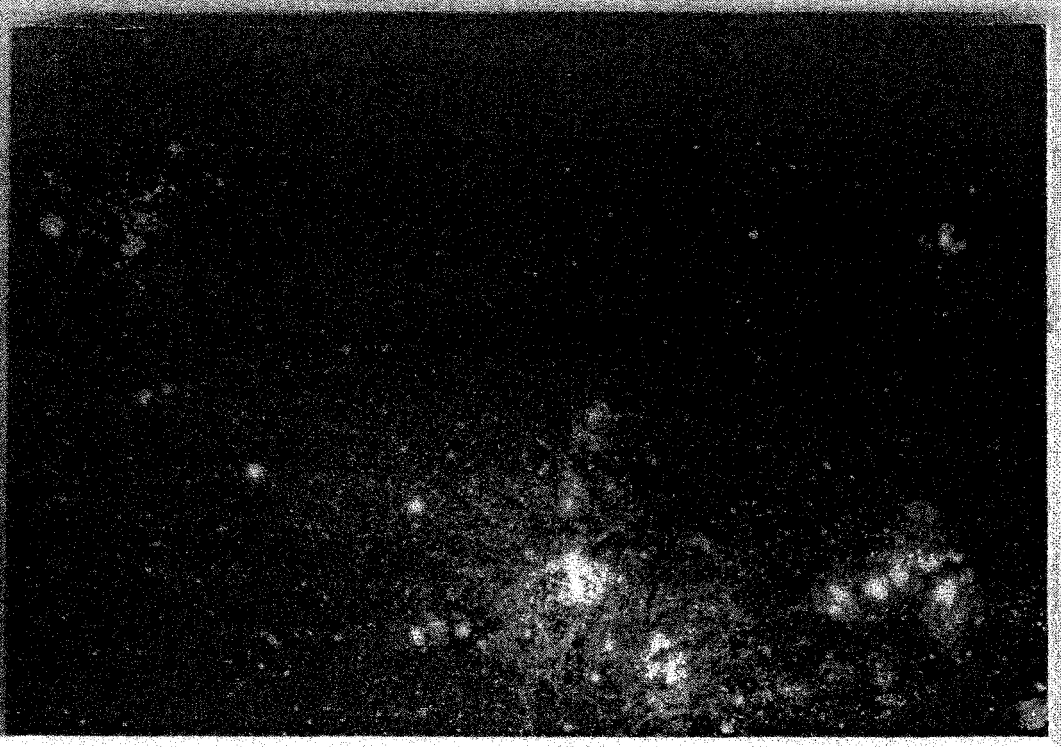

Ed. Arunava Bhadra

Exploring the Cosmos

Proceedings of the Conference on Astrophysics and Astroparticle Physics held at NBU during Jan 27 & 28, 2011

LAP LAMBERT Academic Publishing

Impressum/Imprint (nur für Deutschland/ only for Germany)
Bibliografische Information der Deutschen Nationalbibliothek: Die Deutsche Nationalbibliothek verzeichnet diese Publikation in der Deutschen Nationalbibliografie; detaillierte bibliografische Daten sind im Internet über http://dnb.d-nb.de abrufbar.

Coverbild: www.ingimage.com

Verlag: LAP LAMBERT Academic Publishing GmbH & Co. KG
Dudweiler Landstr. 99, 66123 Saarbrücken, Deutschland
Telefon +49 681 3720-310, Telefax +49 681 3720-3109
Email: info@lap-publishing.com

Herstellung in Deutschland:
Schaltungsdienst Lange o.H.G., Berlin
Books on Demand GmbH, Norderstedt
Reha GmbH, Saarbrücken
Amazon Distribution GmbH, Leipzig
ISBN: 978-3-8443-9165-7

Imprint (only for USA, GB)
Bibliographic information published by the Deutsche Nationalbibliothek: The Deutsche Nationalbibliothek lists this publication in the Deutsche Nationalbibliografie; detailed bibliographic data are available in the Internet at http://dnb.d-nb.de.

Cover image: www.ingimage.com

Publisher: LAP LAMBERT Academic Publishing GmbH & Co. KG
Dudweiler Landstr. 99, 66123 Saarbrücken, Germany
Phone +49 681 3720-310, Fax +49 681 3720-3109
Email: info@lap-publishing.com

Printed in the U.S.A.
Printed in the U.K. by (see last page)
ISBN: 978-3-8443-9165-7

Gamma-Hadron discrimination of primary cosmic rays from EAS observations

R. K. Dey

Department of Physics, University of North Bengal, Siliguri, WB INDIA 734013

rkdey2007phy@rediffmail.com

A. Bhadra

High Energy & Cosmic Ray Research Centre, University of North Bengal, Siliguri WB INDIA 734013

aru_bhadra@yahoo.com

A Monte Carlo simulation study has been carried out, aimed at identifying and rejecting the background component, constituted by hadronic cosmic rays, from γ-ray primaries at energies above 100 TeV. The usual methods for this purpose using muons and secondary hadrons are revisited here. In this work our main focus is to discuss the possible role of longitudinal age, lateral age and local age parameters of EAS for separating γ-ray initiated showers from hadronic showers. Local age parameter may serve as an estimator of gamma-hadron discrimination in ground-based EAS experiments with or without muon measurement facilities.

Pacs: 96.50.sd, 96.50.sb, 95.75.-z, 96.50.S-

Keywords: cosmic ray, EAS, gamma-hadron, Monte Carlo simulations

1. INTRODUCTION

The present astrophysical conjecture of γ-ray astronomy is leading to answer several questions related with the origin and acceleration mechanisms of Cosmic Rays. This becomes a viable branch of main stream astronomy with the advent of the ground-based imaging Cherenkov telescopes. The Cherenkov telescopes HESS, VERITAS and the Fermi γ-ray satellite along with CGRO produce results which agree remarkably well with theoretical predictions [1]. To understand the important

features of the primary energy spectrum vis-a-vis the chemical composition of the cosmic rays at UHE and extremely high energy, a complete study of cosmic ray air-shower has been the only feasible way. The direct measurements of primary cosmic ray flux nearly 10^{14} eV and above are impractical because of very low and sharply falling flux, but has to be inferred from observations of extensive air showers.

The EAS measurements provide various observable parameters namely shower size (N_e), muon size (N_μ), lateral age ($s_\square$), local age (s_{Local}), hadron number (N_{Had}), air shower associated Cherenkov photons (N_{Ch}), shower maximum (X_{max}) and longitudinal age (s_L) (where air-shower arrays are equipped with fluorescence detectors [2,3]) and many of these observables are found to be sensitive to primary masses with different degrees. The measurements from different experiments would still require detailed Monte Carlo simulations of the shower development as a basis of the data analysis and interpretation. The M C simulations consider the evolution of EAS in the atmosphere initiated by different energetic particles. Modern air-shower arrays equipped with large area detectors and improved electronics could precisely measure several EAS components simultaneously [4,5]. Currently simultaneous observations of showers using two distinct detector methods could also help to limit systematic errors that have inundated cosmic ray experiments.

In the field of cosmic ray physics, the discrimination of γ-ray induced air showers from hadron-induced air showers is a long standing problem that still needs more attention [6,7,8]. γ-ray detection suffers from the huge background constituted by ordinary cosmic rays (hadrons), whose flux is about 4 order of magnitude larger than the γ-ray flux. To observe astrophysical sources (assume as point-like objects), one has to eliminate isotropically distributed cosmic rays. In this paper we will discuss some important distinguishing features of γ-ray induced EASs from those induced by the normal cosmic ray nuclei with the help of age parameters & few

other best possible EAS observables. In EAS technique the muon measurements of the two types of showers are important because muon content has been treated beautifully as one of the primary mass sensitive parameters. In KASCADE experiment the secondary hadron content has been used in order to distinguish different primary cosmic ray nuclei but measurements were at variance with the results obtained from electron/muon analysis at sea level [9]. The hadron measurements are usually preferable at mountain altitude because of higher EAS survival energy in the form of hadron component. The three different shape parameters ($s_{\square}$, s_{Local} & s_L) of their lateral and longitudinal profiles of simulated EASs are used in this work to extract important distinguishing features between γ-ray induced showers and protons/nuclei induced showers.

The important considerations adapted in the simulation procedure are given in section **II**. The three different shower age parameters are described briefly in section **III**. In section **IV** we discuss the results obtained on gamma-hadron separation. Finally, section **V** presents our conclusions.

2. SIMULATIONS OF EAS

Results for the present work have been obtained by coupling the high energy (above 80 GeV/n) hadronic interaction model QGSJet 01 version 1c [11] and the low energy (below 80 GeV/n) hadronic interaction model GHEISHA (version 2002d) [12] in the framework of the CORSIKA Monte Carlo program version 6.600 [10]. For the electro-magnetic part the EGS4 [13] program library simultaneously with the NKG option has been used.

The US-standard atmospheric model [14] with planar approximation has been considered which works only for the zenith angle of the primary particles being less than 70°. The maximum primary zenith angle has been restricted to 45° here. The

EAS events initiated by primary protons as well as Iron nuclei and γ-ray have been simulated. The Monte Carlo simulation data library consists of 40,000 EAS events for each primary component p, He, Fe and γ-ray in the primary energy range from 10^{14} eV to $3x10^{16}$ eV followed a power law with a spectral index of -2.7 . A mixed sample has also been prepared from the generated showers taking 50% p, 25% He and 25% Fe events for better understanding of EAS observational results. We simulated EAS events based on the characteristics of several air shower arrays such as NBU, ARGO-YBJ, KASCADE and MT. CHACALTAYA. The magnetic fields are set accordingly. On ground level the kinetic energy thresholds are chosen as 50 MeV, 50 MeV, 3 MeV and 3 MeV for secondary hadrons, muons, photons and electrons.

3. SHOWER AGE PARAMETERS

According to the cascade theory, the developmental stage of a pure electromagnetic cascade can be expressed by a single parameter s_L, known as longitudinal shower age. This parameter is determined as the saddle point in the inverse Melline transformation of cascade transport equation. In approximation B, it is possible and natural to consider the value of s_L as

$$s_L = \frac{3t}{t+2ln\frac{E_O}{\epsilon_o}} \qquad (1)$$

where t is the (slant) atmospheric depth of observational level, E_o is the energy of the primary photon/electron, ϵ_o is the critical energy (in air $\epsilon_o \approx 81$ MeV).

Recent Monte Carlo simulation studies demonstrated universality for large EAS with primaries in the EeV energy range in terms of longitudinal age defined through the relation

$$s_L = \frac{3t}{t+2t_{max}} \qquad (2)$$

where t_{max} is the depth of the shower maximum. The longitudinal data sub-block of CoRSiKa output provides t and t_{max} for estimating s_L.

In the same theoretical framework Nishimura and Kamata solved numerically the 3-dimensional shower equations in approximation **B** to obtain the lateral distribution of electrons progressing in a constant medium. The density profile of cascade electrons was fitted by Greisen with the approximate form called NKG structure function, given by

$$\rho(r, s_{\square}) = N_e c(s_{\square})(\frac{r}{r_m})^{s_{\square}-2}(1+\frac{r}{r_m})^{s_{\square}-4.5} \quad (3)$$

where r_m is the Moliere radius which takes different values for different sites and $c(s_{\square})$ is a normalization factor.

$$c(s_{\square}) = \frac{\Gamma(4.5-s_{\square})}{2\pi r_m^2 \Gamma(s_{\square})\Gamma(4.5-2s_{\square})} \quad (4)$$

To obtain $s_{\square}$ the standard procedure in which simulated electron densities at different radial distances are fitted by the method of Chi-square-minimization through an iterative procedure based on the method of steepest decent to the NKG lateral distribution function [15] of electrons mentioned in equation (3).

For better estimation of shower age from experimental density distribution of electrons, Capdevielle introduced the notion of local age parameter (s_{Local}) [15]. From two neighbouring points, i and j, one can give a lateral age parameter for any distribution f(x) (where $x = r/r_m$) that characterizes the best fit by a NKG-type function in $[x_i, x_j]$:

$$s_{ij} = \frac{\ln(F_{ij}X_{ij}^2 Y_{ij}^{4.5})}{\ln(X_{ij}Y_{ij})} \quad (5)$$

Where $F_{ij} = f(r_i)/f(r_j)$, $X_{ij} = r_i/r_j$ and $Y_{ij} = (x_i+1)/(y_j+1)$. More generally, r_i approaches to r_j, this suggests the definition of the LAP s(x) (s(r)) at each point:

$$s(r) = \frac{1}{(2x+1)}\left((x+1)\frac{\partial lnf}{\partial lnx} + (2+\beta_o)x + 2\right) \quad (6)$$

If β_o =4.5, $f_{NKG}(r)$ with s=s(r) can be used to fit f in the neighbourhood of r. The identification $s(r)= s_{ij}$ for $r = (r_i+r_j)/2$ remains valid for the experimental distributions as long as they are approximated by monotonic decreasing functions versus distance: A typical behaviour of s(r) was inferred with a characterized minimum value of the parameter near 30-50 m from the axis followed by a general increase up to 300 m and again showing a decrement beyond it. A single average age parameter was estimated taking average of all local ages measured in different radial bands between first minima (45 m) and subsequent maxima (200 m) to incorporate important properties of shower initiating particles into it.

4. RESULTS ON GAMMA-HADRON SEPARATION

Based on Monte Carlo simulation studies, some important distinguishing characteristics of hadron and γ-ray initiated air showers have been investigated. The various observable parameters like shower size (N_e), muon size (N_μ), hadron number (N_{Had}), longitudinal age (s_L), lateral age ($s_\square$), local age (s_{Local}) and average age (s_{av}) are being used for this study.

A. ELECTRON-MUON AND ELECTRON-HADRON CO-RELATIONS

The average number of muons and secondary hadrons against the number of electrons are depicted in figures 1a and 1b. It could clearly be recognized that curves for hadron primaries are well above from that for the gamma-ray in both figures. For extensive air shower arrays examining higher energy regions for the selection of primary γ-ray (typically greater than 100 TeV or so), rejection of hadronic background based on the measured muon content remains a promising technique [17]. However, this technique becomes inefficient in regimes where the

expected muon number for protons/nuclei initiated showers is low due to lower primary energy and/or with wider geometrical spread in the shower profile. In such a situation protons/nuclei initiated showers are eliminated from γ-ray showers through the estimation of EAS events which are `secondary hadron-rich' with respect to the number of hadrons expected from γ-ray initiated showers [18].

B. VARIATION OF s_L WITH N_e

The penetration of the atmospheric matter by EASs is determined generally by the elasticity of the interaction defined as the fraction of energy carried by the leading secondary particle. The EASs initiated by γ-rays have large elasticity values compared to hadron initiated showers and by this reason the γ-ray induced showers penetrate more in the atmosphere, as can be distinguished from the comparison of their longitudinal ages [19]. In figures 2a and 2b, we have presented the results obtained on this feature corresponding to the photonic and the nucleonic origin of primary particles at three different depths.

C. N_e & N_μ DEPENDENCIES OF MEAN $s_\perp$

The correlation between mean lateral shower age and shower size in the shower size range (10^3 - 1.5 x 10^6) with the zenith angle interval (0° - 45°) for p, Fe, γ, mixed composition using QGSJet model and NBU results are put on view in figure 3b. It is important to perceive that the lateral shower age takes higher values for heavy nuclei compare to that of light and γ-ray primaries clearly indicating relatively flatter lateral distribution of electrons as one starts from gamma to Fe via p.

The variation of mean lateral shower age parameter with muon size in the primary energy range (10^{14}-3x10^{16} eV) in the zenith angle interval 0° - 45°) for p, Fe, γ-ray primaries is presented in figure 3a with Kascade data. The variation exhibits the same nature as obtained in the KASCADE experiment using NKG fitting for muons with slightly higher muon threshold energy [20]. The figure also exposes the fact

that γ-ray initiated showers are easily distinguishable from hadron showers in terms of s and N_μ but the discrimination between lighter and heavier hadrons at higher energies becomes gradually inappropriate. From our earlier simulation study it has been concluded that EASs from light primary components are younger in average.

D. RADIAL DEPENDENCE OF LOCAL AGE & DISTRIBUTION OF S_{av}

Using equation (5) we have studied the radial dependence of the local age (s_{Local}) for six different Moliere radii between 10-200 m for p, Fe and γ-ray primaries at Kascade site with different primary energies (figures 4a, 4b, 4c). The nature of variations of s_{Local} are almost identical irrespective of primary energy and mass. This behavior of the local age parameter leads to exhibit some kind of scaling feature of radial electron distributions. The radial variation of s_{Local} for p, Fe and γ, at three different altitudes (Kascade, Argo and Mt. Chacaltaya) are shown in figures 5a, 5b, 5c and they exhibit a very good indication of gamma-hadron separation. A very little shift of minima points is observed in s_{Local} vs r plot (figure 6) keeping overall shape unaltered for different altitudes. In figure 7 we have shown the frequency distributions of the estimated average age (s_{av}) and the early development of γ-ray initiated shower compare to hadron showers is revealed from it.

5. CONCLUSIONS

A simulation study has been made to separate the background cosmic rays constituted by hadrons from γ-ray primaries at energies above 100 TeV at four geographical sites. Our conclusions are as follows:

1. The well established fact that muons have higher discriminating power between γ-ray and hadron rather than secondary hadrons is verified once again.

2. It has been recognized from our present simulation study that γ-ray initiated showers are little younger than hadron showers of the same primary energy, zenith angle and observational level.

3. The longitudinal age parameter s_L could be useful for gamma-hadron separation for EAS experiments those equipped with optical detectors (CT & FD).

4. The experimental profiles of EAS cannot be expressed in terms of NKG function with a single age parameter. Consequently, though the lateral age parameter contains information of both hadronic cascading and primary composition, its determination can be biased while fitting the experimental distributions. The characteristic dependence of local age parameter with radial distance allows a more accurate determination of $s_{\square}$.

5. The lateral distribution of electrons in EAS exhibits some sort of scaling (energy, mass independent) behaviour in terms of the local age parameter at least in the energy range 100 TeV to 1 EeV and in few sites in the altitude range 110 m to 5300 m (however a little shift of minima in s_{Local} with altitude is noticed).

6. The local age parameter qualifies reasonably well as an estimator for gamma/hadron discrimination and may separate γ-ray showers from the hadronic background where muon measurements are not made (but array should be densely packed for precise density measurement i.e. ARGO-YBJ). On the other hand, s_{Local} may also be used simultaneously with N_μ in experiments such as GRAPES-3 with concurrent muon measurement facility.

7. The frequency distributions of s_{av} for p, Fe and γ-ray initiated showers exhibit a distinguishing character between γ-ray and hadron primaries.

ACKNOWLEDGEMENT

The authors are thankful to Professor J. N. Capdevielle from the University de Paris for several fruitful discussions. A. Bhadra would like to thank the Department of Science and Technology (Govt. of India) for support under the grant no. SR/S2/HEP-14/2007

REFERENCES

1. F Acero et al., HESS collaboration, http://arxiv.org/abs/0909.4651; V A Acciari et al., VERITAS collaboration, http://arxiv.org/abs/0911.0873 and A Abdo et al., Fermi collaboration, Astron., in press.
2. D J Bird et al. (Fly's Eye collaboration), Phys. Rev. Lett. 71, 3401 (1993).
3. R U Abbasi et al., (HIRES collaboration), Astrophys. J, 622, 910 (2005).
4. M Aglietta et al., Astropart. Phys. 20, 641 (2004).
5. T Antoniet al., Astro-ph/0505413, To appear in Astropart. Phys. (2005).
6. T Gaisser, Cosmic Rays and Particle Phys., Cambridge University Press. Oxford 1990.
7. S Nestnhoff et al., Astropart. Phys.4 (1995) 119-132.
8. H M Badran, T C Neekes, Astropart. Phys. 7 (1997) 307-314.
9. Engel J et al., 1999 Proc. 26th Int. Cosmic Ray conf. vol1, p349.
10. D. Heck et al., FZKA-Report 6019, Forschungszentrum Karlshruhe, (1998).
11. J N capdevielle and P Gabinski, J Phys G. Nucl Part. 16, 769 (1990).
12. H Fesefeldt Report PITHA-85/02 (RWTH Aachen) (1985).
13. W R Nelson, H Hiramaya, D W O Rogers, Report SLAC 265, (1985).
14. National Aeronautics and Space Administration (NASA), U.S. Standard Atmosphere, Tech. Rep. NASA-TM-X-74335 (1976); J Knapp, and D Heck, Tech. Rep. 5196B, Kernforschungszentrum Karlsruhe (1993).
15. K Greisen, Ann. Rev. of Nucl. and Part. Science, 10, 63 (1960).
16. Capdevielle J N, Gawin J and Procureur J 1978 J. Phys. G:Nucl. Phys. 4, 303; 1977 15th ICRC, Plovdiv 8 341.
17. T Stanev, T K Gaisser and F Halzen, Phys. Rev. D, 32, 1244 (1985).
18. Danilova T V et al., 1985, Proc. 19th ICRC 2, 260.
19. H J Drescher and G R Farrar, Phys. Rev. D 67, 116001 (2003).
20. T Antonio, et al., Astropart. Phys. 14, 245 (2001).

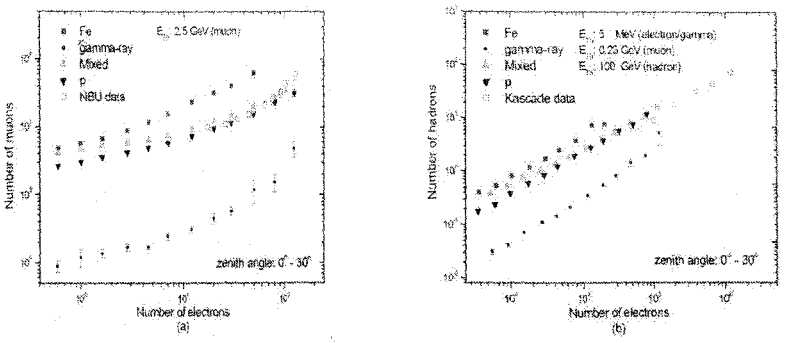

FIG.1: Number of muons[a] and hadrons[b] as a function of electron numbers for p, Fe, γ-ray, mixed composition and experimental data. Our simulated results with initial set of different threshold energies have been reduced to desired values through simulation as demanded for comparison with experiments.

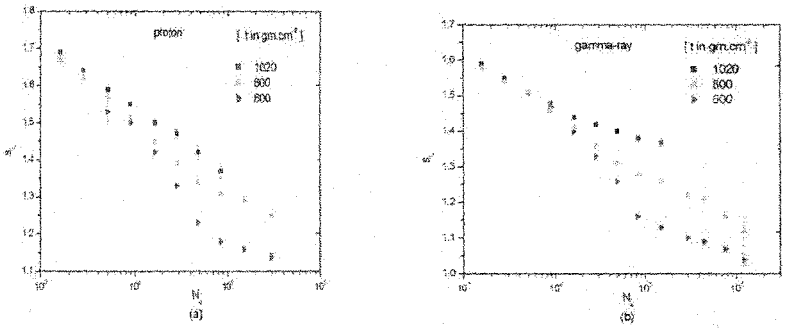

FIG.2: Variation of longitudinal shower age with shower size at three different atmospheric depths for CORSIKA generated simulated showers: [a] proton and [b] gamma-ray.

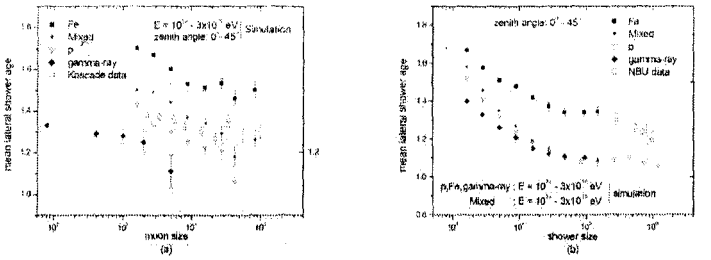

FIG.3: [a] Variation of mean lateral shower age with muon size. [b] Variation of mean lateral shower age with shower size along with NBU data. For comparison with Kascade data in Figure a, where the age parameter was estimated by NKG fits with r_μ as 420 m and also used truncated muon sizes N_μ^{tr}.

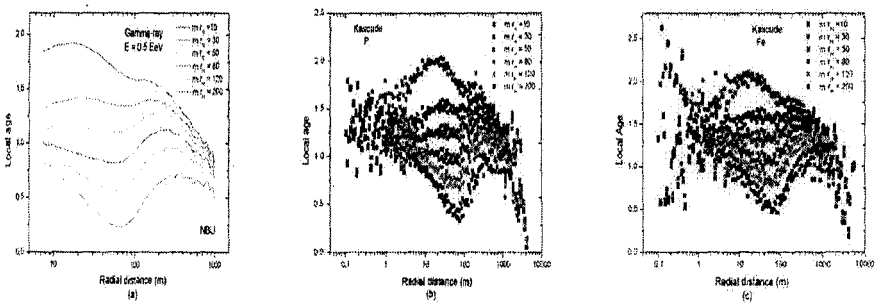

FIG.4: Local age parameter for different Moliere radii.

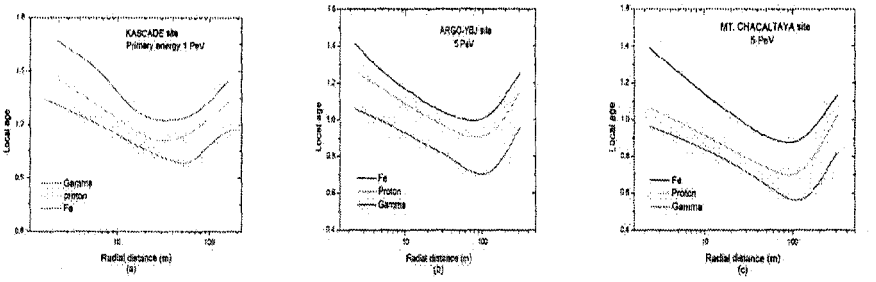

FIG.5: Local age parameter behaves as a good indicative parameter of gamma/hadron discrimination in different sites.

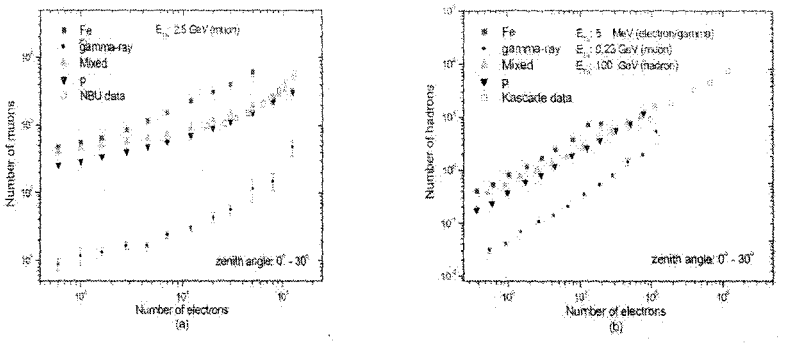

FIG.1: Number of muons[a] and hadrons[b] as a function of electron numbers for p, Fe, γ-ray, mixed composition and experimental data. Our simulated results with initial set of different threshold energies have been reduced to desired values through simulation as demanded for comparison with experiments.

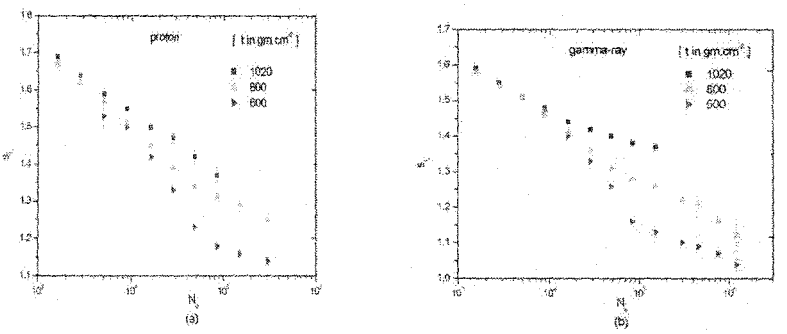

FIG.2: Variation of longitudinal shower age with shower size at three different atmospheric depths for CORSIKA generated simulated showers: [a] proton and [b] gamma-ray.

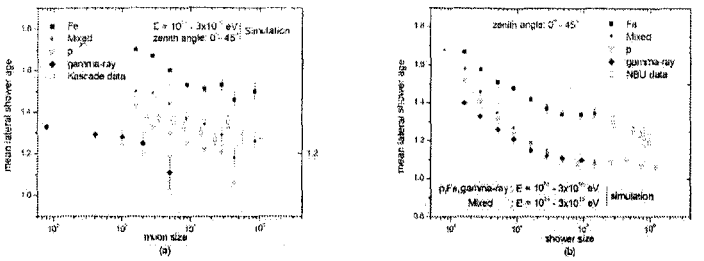

FIG.3: [a] Variation of mean lateral shower age with muon size. [b] Variation of mean lateral shower age with shower size along with NBU data. For comparison with Kascade data in Figure a, where the age parameter was estimated by NKG fits with r_μ as 420 m and also used truncated muon sizes N_μ^{tr}.

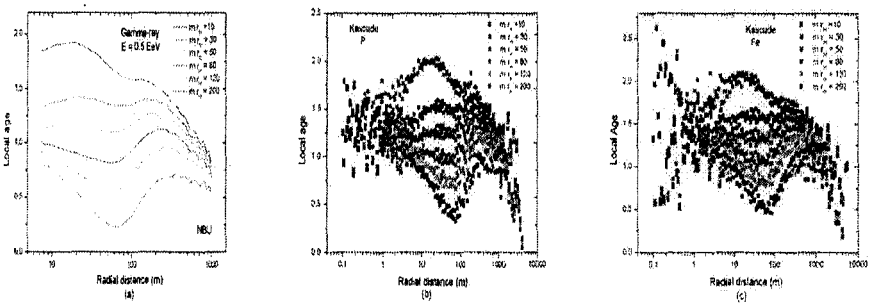

FIG.4: Local age parameter for different Moliere radii.

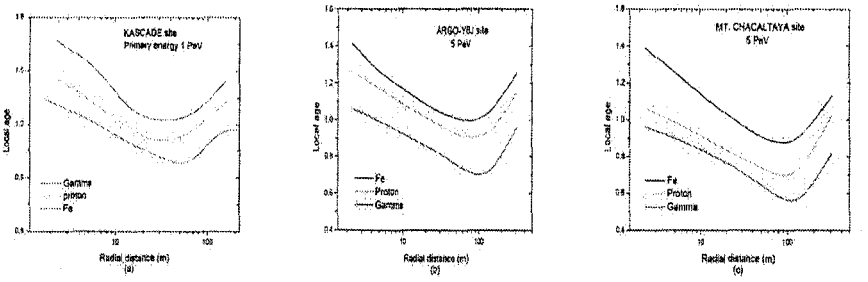

FIG.5: Local age parameter behaves as a good indicative parameter of gamma/hadron discrimination in different sites.

Behaviour of the EAS Age Parameter in the Knee Energy Region

R.K. Dey
Dept of Physics, Univ. North Bengal, Siliguri, WB 734013 India

A. Bhadra
High Energy & Cosmic Ray Research Ctr, Univ. North Bengal, Siliguri, WB 734013 India

J.N. Capdevielle
APC, Univ.Paris Diderot, 10 rue A.Domon, 75205 Paris, France

Analyzing simulated EAS events generated with the CORSIKA code, the characteristics of lateral distribution of electrons in EAS around the knee energy region of the primary energy spectrum have been studied and compared with experimental observations. The differences between the EGS4 and the NKG output of CORSIKA in respect to electron radial density distribution have been investigated. The relation between lateral and longitudinal age parameters has been studied after introducing the notion of the local age parameter that reflects the profile of the lateral distribution of electrons in EAS. The present analysis motivates the inclusion of the lateral shower age in a multiparameter study of EAS to extract information on hadronic interactions and primary composition.

I. THE DIFFERENT AGE PARAMETERS

The concept of shower age was introduced in cascade theory to describe the stage of development of an electromagnetic (e.m.) cascade. A synthesis summarizing the works of Greisen and Nishimura-Kamata under Approximation B of cascade development [1] in respect to shower age is the following: the longitudinal age s_L is defined here as

$$s_L = \frac{3t}{t + 2ln(E/\epsilon_0)} , \qquad (1)$$

where E_0 is the energy of the primary photon generating the cascade, t is the atmospheric (divided by the electron radiation lenth in air taken as 37.1 g-cm^{-2}), ϵ_0 being the critical energy of 82 MeV.

In this theoretical context the lateral density distribution of cascade particles given by Nishimura and Kamata can be approximated by the well known Nishimura-Kamata-Greisen (NKG) structure function,

$$f(r) = C(s_\perp)(r/r_m)^{s_\perp - 2}(1 + r/r_m)^{s_\perp - 4.5} , \qquad (2)$$

where r is the radial distance measured from the EAS core, r_m is the Moliere radius, $s_\perp$ is the lateral age : the normalization factor C($s_\perp$) is given by

$$C(s_\perp) = \frac{\Gamma(4.5 - s_\perp)}{2\pi\Gamma(s_\perp)\Gamma(4.5 - 2s_\perp)} . \qquad (3)$$

implying that for the density $\rho_{NKG}(r) = N_e f(r)$ thanks to the properties of the Eulerian function.

The relation $s_L = s_\perp$ was initially considered to hold for pure e.m. showers and it was admitted that the average steepness of the profile of the lateral distribution has a correlation with the longitudinal development.

Later the 3D diffusion equations were solved again by Uchaikin and Lagutin using adjoint equations and an improvement of NKG function was proposed by modulating r_m to s_L as follows:

$$\rho_{el}(r) = (mr_m)^{-2}\rho_{NKG}(r/m) \qquad (4)$$

with $m = 0.78 - 0.21s_L$.

The validity of this approach was demonstrated [3] by pointing out that the experimental distributions in EAS are steeper than the ρ_{NKG} but are in better agreement with Monte Carlo calculations of Hillas.

For better estimation of shower age from the experimental distributions, one of us (Capdevielle) introduced the notion of the local age parameter (LAP) s_{Loc} [3]: From two neighbouring points, i and j, one can give a lateral age parameter for any distribution $f(x)$ (where $x = \frac{r}{r_m}$) that characterises the best fit by a NKG-type function in $[x_i, x_j]$:

$$s_{ij} = \frac{\ln(F_{ij}X_{ij}^2Y_{ij}^{4.5})}{\ln(X_{ij}Y_{ij})} \qquad (5)$$

where $F_{ij} = f(r_i)/f(r_j)$, $X_{ij}=r_i/r_j$, and $Y_{ij}=(x_i+1)/(x_j+1)$. More generally, if $r_i \to r_j$, this suggests the definition of the LAP $s(x)$ (or $s(r)$) at each point :

$$s(r) = \frac{1}{2x+1}\left((x+1)\frac{\partial \ln f}{\partial \ln x} + (2+\beta_0)x + 2\right) \qquad (6)$$

If β_0=4.5, $f_{NKG}(r)$ with s=$s(r)$ can be used to fit f in the neighbourhood of r.

The identification $s(r) = s_{ij}$ for $r = \frac{r_i + r_j}{2}$ remains valid for the experimental distributions as long as they are approximated by monotonic decreasing functions versus distance: A typical behaviour of s(r) was infered with a characterised minimum value of the parameter near 30 – 50 m from the axis followed by a general increase at large distance and it suggests a relation $s_L \sim 1.25 - 1.3 s_\perp$.

After verification of the behaviour of the LAP through experimentally observed lateral distributions and particularly a detail study of the parameter with the Akeno data [4], this approach was validated by the rapporteurs of the ICRC from 1981 to 1985 [5]. This procedure was also used in extension to calculate the radio effect of very large EAS [6].

II. 3D SIMULATION OF EAS

In the present work, the high energy (above 80GeV/n) hadronic interaction model QGSJET 01 version 1c has been used in combination with the low energy (below 80GeV/n) hadronic interaction model GHEISHA (version 2002d) in the framework of the CORSIKA Monte Carlo program version 6.600 [7] to generate EAS events. The simulated shower library produced consists mainly of 10,000 EAS for each primary species Proton, Helium and Iron in the primary energy interval of 10^{14} eV to 3×10^{16} eV.

Taking the opportunity of calculating simultaneously the e.m. component via both the options, the EGS and the NKG option (implemented following [3] by exploiting the relation (4) in the subcascades treatment) as admitted in CORSIKA package, we have carried out parallel simulations. We ascertain that when the calculation of the electron component is carried out with relation (4), the situation with the NKG inspired procedure implemented in CORSIKA is more close to the experimental data and also to the calculation with the EGS, as shown in fig.1. The NKG option gives a slighly larger density with steeper radial distribution in compare to the EGS option. A small density excess appears for pure electromagnetic cascades near the axis for the Corsika NKG option. Such an excess appears also in proton induced air showers. However, over a large band of densities between the radial distance $10m$ up to $100m$ from the axis, a tolerable agreement is noticed.

For Fe primaries, both the options produce older profile near the axis with density excess (particularly in the case of NKG option) between $2 - 10m$ distance. The average energy of the positrons is quite small in the case of iron initiated showers and the cross section of positron annihilation becomes more important for the lower part of the cascade. This effect is probably enhanced by the longer path of the electrons in the geomagnetic field (and larger energy loss by ionisation). Therefore the NKG option is not a very good option

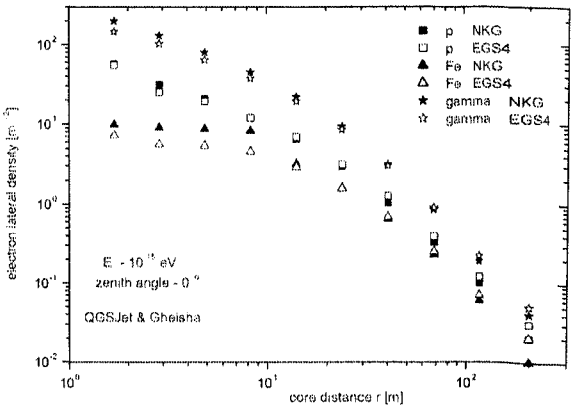

FIG. 1: Comparison of radial distribution of electrons for CORSIKA NKG and EGS options for proton and Fe primaries.

for the simulation of heavy nuclei initiated inclined showers after the maximum development of cascade. Near vertical showers in low altitudes are nevertheless acceptable. Conversely for very high energy primaries the average energy of the positrons remains important and for proton and photon showers NKG option is still useful to calculate a large number of cascades in a short time.

At larger distances a slight deficit in densities appears with the NKG option; it seems to come from the different treatment of the multiple coulomb scattering in the EGS and also may due to the enhanced path of the muons in the geomagnetic field which results in greater loss of energy by ionisation and subsequently their decay produces more electrons. The EGS takes into account the photoproduction inside the e.m. subcascades.

Through a smaller sample of events simulated in the energy band $10^{18} - 10^{20}$eV [9], we have also observed that the lateral distributions calculated at distances lower than 300m from the axis with the NKG option as well as the total longitudinal development do not differ much from those obtained with the EGS. Consequently, the NKG option in CORSIKA remains useful for faster calculations at ultra high energy initiated by a nucleon or nuclei. This circumstance allows the calculation of radio effect as in [6] as well as the fluorescent component via the NKG option. The Landau Pomeranchuk Migdal effect (LPM)(not included in the NKG option) limits however the employment of the option beyond 10^{18}eV for γ primaries.

The fluctuations in lateral shower age are much larger for proton initiated showers compared to those initiated by heavier primary.

This distribution (fig.2) can be fitted by an Extreme

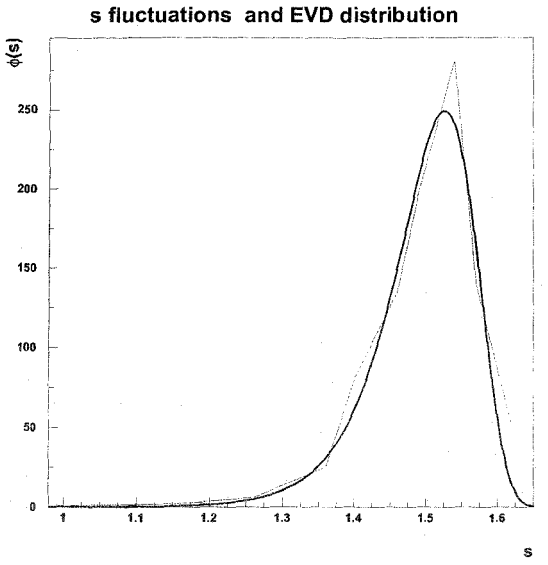

FIG. 2: fluctuation of shower age at fixed shower size $N_e = 10^4$ fitted by an E.V.D. function $\phi(s)$ (vertical showers, sea level, p primaries)

Value Distribution (E.V.D) defined through

$$\phi(s) = \frac{1}{\sigma} \exp(\pm\frac{\mu - s}{\sigma} - e^{\pm\frac{(\mu-s)}{\sigma}}) \qquad (7)$$

where the parameters μ and σ are related to the average size $\overline{s}$ and its variance V_s by $\overline{s} = \mu \pm 0.577\,\sigma$ and $V_s = 1.645\sigma^2$ (in the case of the histogram of fig.2, $\overline{s} = 1.495$ and $\sigma = 0.07$).

Comparing the results of the EGS and the NKG options with Kascade data [8] in the bin $Log(N_e)[3.9, 4.3]$, we observe that there are small discrepancies in densities even with the Lagutin NKG modified formula taking $s = 1.404, N_e = 11829$ as shown on fig.3

Those mentioned parameters (for Lagutin formula (4)) corresponds respectively to the average lateral age parameter and the average size in the size bin considered (calculated with the size spectrum in Karlsruhe).

III. LAP AND N_e DEPENDANCE

The dependance of the local age parameter $s(r)$ on lateral distance exhibits the typical dependance at the level of Akeno experiment with a minimum near 30-40 m distance and larger values near at small radial distances or at large distances from the axis. An example

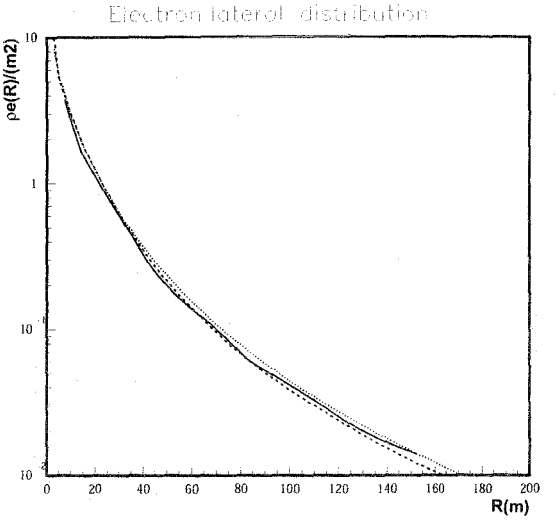

FIG. 3: Lateral electron distributions at Kascade level. Experimental(full line), NKG option(dashed), NKG-Lagutin modified function dotted

is given in the fig.4 for $N_e = 10^6$.

The comprehensive dependance of the lateral age parameter s on N_e is shown on fig.5

The lateral age parameter is obtained as the value of the l.a.p. s(r) averaged inside the shower disc up to the shower radius R_{lim} (distance where the average lateral distribution reaches a threshold density satisfying the trigger conditions and remains detectable by the scintillator detector used i.e. for instance $1el/m^2$ for a counter of $1m^2$ area). One of the most simple interpretations of the minimum near the knee on fig.5 could be a mixed component progressively enriched in nuclei after the knee as suggested half a century ago by the galactic leakage, according to the different Larmor radius of nucleons and heavier nuclei. However, for small energies the shower radius R_{lim} is lower than 40m whereas it exceeds 100m at large energies above the knee; the calculation of the average $s_\perp$ up to those different limits may be the reason for decreasing s below the knee and an increase in age beyond the knee.

IV. CONCLUSION

The experimental profiles cannot be expressed in terms of NKG function with a single age parameter. Consequently, though the lateral age parameter contains information of both hadronic cascading and primary composition, its determination can be biased while fitting the experimental distributions. The char-

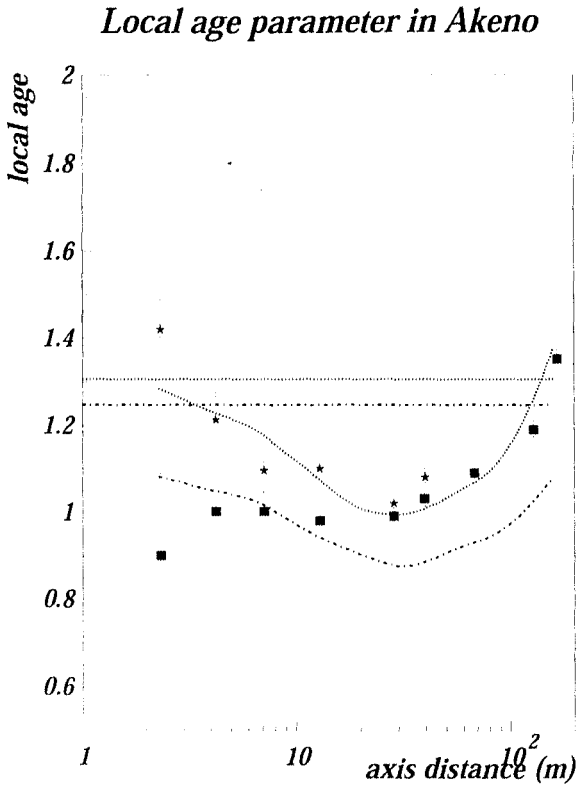

FIG. 4: Local age parameter versus distance at Akeno. Experimental points squares (thick scintillators), stars (thin scintillators), dotted line proton primaries, dashed line iron primary, horizontal lines longitudinal age parameter respectively for p and iron

acteristic dependance of local age parameter with radial distance allows a more accurate determination of $s_\perp$ as well as the conversion to s_L

A detailed study of dependence of $s_\perp$ on shower size, included in a multiparameter analysis (muon-electron abundance, absorption length) and comparison with the Akeno and the Kascade data (in progress) should help to understand the knee region in terms of primary composition.

Acknowledgments

AB would like to thank the DST (Govt. of India) for support under the grant no. SR/S2/HEP-14/2007

[1] G. Cocconi, Cosmic Rays, Handbuch der Physik, 46-1, 215, Berlin: Springer Verlag (1961) and references herein
[2] J. Nishimura, Cosmic rays, Handbuch der Physik, 46, 2,114, Berlin: Springer Verlag, (1967)
[3] J.N. Capdevielle and J. Gawin, J. of Physics G,8, 1317 (1982); M.F. Bourdeau, J.N. Capdevielle and J. Procureur, J. Phys.G, 6, 901, (1980); J.N. Capdevielle and F. Cohen, J.Phys. G : Nucl. Part. Phys., 31 (2005), 507-524 and references herein
[4] M. Nagano et al., Journal of the Physical Society of Japan, vol. 53, pp.1667-1681 (1984)
[5] S. Tonwar, Proc. 17^{th} ICRC, Paris, 13, 330 (1981); M. Rao, Proc. 18^{th} ICRC, Bangalore 11 (1983); R. Clay, Proc. 19^{th} ICRC, La Jolla 9, 323(1985)
[6] D. Suprun et al., Astrop. Phys., 20, 157-168(2003)
[7] D. Heck, J. Knapp, J.N. Capdevielle, G. Schatz and T. Thouw, FZK A report-6019 ed. FZK *The CORSIKA Air Shower Simulation Program*, Karlsruhe (1998); J. N. Capdevielle et al. KfK report-4998, ed. KfK *The Karlsruhe Extensive Air Shower Simulation Code CORSIKA*, Karlsruhe (1992)
[8] T. Antoni, et al., Astropart. Phys. 14, 245 (2001)
[9] J.N. Capdevielle et al, 36, J. Phys. G, 075203 (2009)

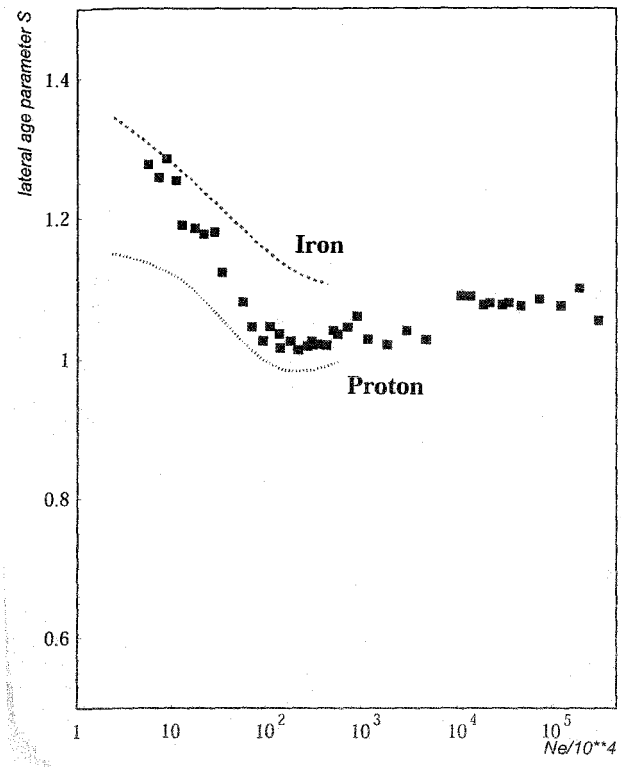

ateral age parameter versus size N_e at Akeno